The Astrophysical Journal, 974:84 (17pp), 2024 October 10 https://doi.org/10.3847/1538-4357/ad6980

What Are the Pillars of Reionization? Revising the AGN Luminosity Function at $z \sim 5$

Andrea Grazian[1], Emanuele Giallongo[2], Konstantina Boutsia[3], Stefano Cristiani[4,5,6], Fabio Fontanot[4,6], Manuela Bischetti[4,7], Laura Bisigello[8], Angela Bongiorno[2], Giorgio Calderone[4], Francesco Chiti Tegli[9], Guido Cupani[4,6], Gabriella De Lucia[4,6], Valentina D'Odorico[4,6,10], Chiara Feruglio[4,6], Fabrizio Fiore[4,6], Giovanni Gandolfi[1,11], Giorgia Girardi[1,11], Francesco Guarneri[4,12], Michaela Hirschmann[4,13], Matteo Porru[4,7], Giulia Rodighiero[1,11], Ivano Saccheo[2,14], Matteo Simioni[1], Andrea Trost[4,7], and Akke Viitanen[2]
[1] INAF–Osservatorio Astronomico di Padova, Vicolo dell'Osservatorio 5, I-35122, Padova, Italy; andrea.grazian@inaf.it
[2] INAF–Osservatorio Astronomico di Roma, Via Frascati 33, I-00078, Monte Porzio Catone, Italy
[3] Cerro Tololo Inter-American Observatory/NSF NOIRLab, Casilla 603, La Serena, Chile
[4] INAF–Osservatorio Astronomico di Trieste, Via G.B. Tiepolo 11, I-34143, Trieste, Italy
[5] INFN-National Institute for Nuclear Physics, Via Valerio 2, I-34127, Trieste, Italy
[6] IFPU–Institute for Fundamental Physics of the Universe, Via Beirut 2, I-34151, Trieste, Italy
[7] Dipartimento di Fisica, Sezione di Astronomia, Università di Trieste, Via G.B. Tiepolo 11, I-34131, Trieste, Italy
[8] INAF–Istituto di Radioastronomia, Via Piero Gobetti 101, I-40129 Bologna, Italy
[9] Università degli Studi di Firenze, Via G. Sansone 1, I-50019 Sesto Fiorentino, Italy
[10] Scuola Normale Superiore, Piazza dei Cavalieri 7, I-56126 Pisa, Italy
[11] Department of Physics and Astronomy, Università degli Studi di Padova, Vicolo dell'Osservatorio 3, I-35122, Padova, Italy
[12] Hamburger Sternwarte, Universitat Hamburg, Gojenbergsweg 112, D-21029 Hamburg, Germany
[13] Institute for Physics, Laboratory for Galaxy Evolution, EPFL, Observatoire de Sauverny, Chemin Pegasi 51, 1290 Versoix, Switzerland
[14] Dipartimento di Matematica e Fisica, Università Roma Tre, Via della Vasca Navale 84, I-00146, Roma, Italy
Received 2024 May 27; revised 2024 July 23; accepted 2024 July 29; published 2024 October 7

Abstract

In the past, high-z active galactic nuclei (AGNs) were given a minor role as possible drivers of reionization, despite initial evidence in favor of their large space densities at low luminosities by Chandra and the Hubble Space Telescope. Recent observations from JWST are finding relatively large numbers of faint AGNs at $z > 4$, convincingly confirming these early results. We present a sample of $z \sim 5$ AGNs, both from wide, shallow ground-based surveys and from deep, pencil-beam observations from JWST, allowing us to estimate their space densities with unprecedented accuracy. The bright end ($M_{1450} < -26$) of the $z \sim 5$ AGN luminosity function is well constrained, with a rather steep slope. The faint end ($M_{1450} \geqslant -22$) indicates a high space density, the scatter is significant, and the knee ($M_{1450} \sim -24$) is mostly undetermined. Comparisons with state-of-the-art models find reasonable agreement with the observed AGN luminosity function at $z = 5$, while the predicted space density evolution at higher redshifts appears to be too fast with respect to observational constraints. Given the large variance at the faint end, we consider different options in fitting the luminosity functions and deriving the ionizing emissivity. Even in the most conservative scenario, the photoionization rate produced by $z \sim 5$ AGNs is consistent with the ultraviolet background measurements. A slow evolution of the space density of faint AGNs is observed, indicating that active SMBHs are probably producing large amounts of ionizing photons at $z > 6$, well into the Epoch of Reionization. This is an important indication that high-z AGNs could be major contributors to the reionization of the Universe.

Unified Astronomy Thesaurus concepts: Observational cosmology (1146); Quasars (1319); Catalogs (205); Surveys (1671); Reionization (1383)

1. Introduction

The Cosmic Dawn marks the renaissance of light, when the first sources of ultraviolet (UV) radiation, after the so-called Dark Ages, were again able to separate electrons from protons, leaving them as free particles. This cosmological phase transition, marking the end of the Dark Ages, has been identified as the Epoch of Reionization (EoR; e.g., Barkana & Loeb 2001; Dayal & Ferrara 2018).

Robust constraints on the beginning of the reionization process have been derived through the analysis of the optical depth τ_e of the cosmic microwave background by the Wilkinson Microwave Anisotropy Probe and Planck, which indicate a relatively late ($z_{\rm reion} < 8$) and quick ($\Delta z_{\rm reion} < 2.8$) reionization transition (George et al. 2015; Planck Collaboration et al. 2020; Reichardt et al. 2021). Additional evidence for a late end (at $z \sim 5.3$) to reionization has been obtained by the fact that excess fluctuations in the Lyα forest persisted until 1.1 Gyr after the Big Bang (Bosman et al. 2022; Zhu et al. 2022; Jin et al. 2023; Spina et al. 2024; Zhu et al. 2024).

One of the most important questions in modern astrophysics is which sources drove cosmic reionization in the early Universe. In general, the astronomical community is currently embarked upon finding the long-sought probes that star-forming galaxies are actually the main sources responsible for hydrogen reionization. The active players causing the cosmic reionization of hydrogen have been mostly identified in relation to star-forming galaxies at high redshift (e.g., Atek et al. 2024; Jung et al. 2024) or discovered while looking for their low-z analogs (e.g., Dayal & Ferrara 2018; Flury et al. 2022a, 2022b). So far, the discussion has been mainly focused on the role played by star-forming galaxies (see, e.g., Mascia et al. 2024,

and references therein), and only a few authors have investigated in detail the possible contribution of bright QSOs and faint active galactic nuclei (AGNs) to the reionization process (e.g., Haardt & Madau 1996; Fontanot et al. 2012; Giallongo et al. 2012; Haardt & Madau 2012; Haardt & Salvaterra 2015; Madau & Haardt 2015; Chardin et al. 2017; Puchwein et al. 2019; Madau et al. 2024), despite some early evidence in favor of a consistent space density of faint AGNs, based on Hubble Space Telescope (HST) and Chandra observations (Giallongo et al. 2015, 2019). Very few exceptions (e.g., Boutsia et al. 2021; Grazian et al. 2022; Fontanot et al. 2023; Grazian et al. 2023) to this mainstream scenario have been provided in recent times, proposing the AGN population as a possible alternative in the cosmic reionization scenario.

Recently, this picture has been substantially revised, thanks to two observational results. New wide ground-based surveys of QSOs (e.g., QUBRICS and RUBICON; Grazian et al. 2022, 2023) provide substantial evidence in favor of a relatively large population of bright ($-28.5 \leqslant M_{1450} \leqslant -26.5$) QSOs at $z \sim 5$. In addition, early JWST observations have prompted a revolution in our understanding of the early Universe by highlighting a large population of faint AGNs at $z > 4$ (Harikane et al. 2023; Kocevski et al. 2023; Larson et al. 2023; Maiolino et al. 2023; Scholtz et al. 2023; Furtak et al. 2024; Greene et al. 2024; Matthee et al. 2024). A significant space density of variability selected AGN candidates at $z > 6$ has been found by Hayes et al. (2024). Few exceptional detections of AGNs at $z > 10$ have been provided by Goulding et al. (2023), Maiolino et al. (2024a), Bogdán et al. (2024), and Kovács et al. (2024), which are suggestive of high space density of active SMBHs even at these early epochs. A straightforward estimation of the contribution of these AGNs to the reionization process, mainly based on the AGN fraction in galaxies derived by recent JWST surveys, has been provided by Madau et al. (2024). A first indication has been given by Harikane et al. (2023) and Maiolino et al. (2023) that these SMBHs are overmassive with respect to the local $M_{\rm BH}$–$M_{\rm star}$ relations; though, these results may be biased by selection effects (see, e.g., Li et al. 2024).

The emergence of an unprecedented population of faint objects at $z > 4$ with broad Balmer lines, compact morphology, and V-shaped spectral energy distribution (i.e., flat in the UV rest frame and steep in the optical rest-frame wavelengths), the so-called "Little Red Dots" or "Little Red Monsters" (and interpreted as probable AGNs at high-z; see, e.g., Kocevski et al. 2023, 2024; Kokorev et al. 2024), added further hints that these faint high-z AGNs could indeed be widespread in the early Universe. The nature of these "Little Red Dots" was not fully understood before the launch of JWST (see, e.g., Fiore et al. 2008), and a few of them were typically misidentified as $z > 12$ galaxies in the first surveys (e.g., Labbé et al. 2023). Evidence in favor of unobscured (Type 1) AGNs powering these "Little Red Dots" comes from the fact that they show broad Balmer lines, blue (flat) UV continuum, compact morphology without any visible hosting galaxy, and small attenuation (e.g., Killi et al. 2023) given the observed Balmer decrement of the narrow-line component (but see Pérez-González et al. 2024 for a different interpretation on the nature of the Little Red Dots based on deep MIRI observations with JWST). Interestingly, the contribution of a large population of faint AGNs at $z > 4$, reaching up to $z \sim 10$ and even beyond (e.g., Fujimoto et al. 2023; Goulding et al. 2023; Maiolino et al. 2024a; Habouzit 2024; Hegde et al. 2024; Kovács et al. 2024) could also help to explain the excess of bright ($M_{\rm UV} \sim -20$) primeval ($z > 8$) galaxies recently found by JWST at these high-z by, for example, Naidu et al. (2022), Adams et al. (2024), Chemerynska et al. (2024), and Finkelstein et al. (2024), relaxing the claims of possible tensions of these observations with the Lambda cold dark matter (ΛCDM) standard cosmological model. Indeed, Chworowsky et al. (2024) showed that, taking into account the contamination by AGNs and with a modest change to star formation efficiency, the tension with modern cosmology can be significantly reduced, without invoking ad-hoc scenarios (e.g., Ferrara et al. 2023) or photon budget crisis (e.g., Muñoz et al. 2024). Hidden high-z AGNs in the form of Little Red Dots could also explain the excess of massive galaxies in the galaxy stellar mass functions at $z \sim 10$ (Harvey et al. 2024).

Constraining the AGN luminosity function at $z > 4$ is of utmost importance not only for reionization, but also to find hints about the origin of the large SMBHs discovered at the highest redshifts and the processes governing their growth (e.g., Trinca et al. 2022; Fontanot et al. 2023). Different predictions for the AGN space density as a function of luminosity at $z > 4$ have been derived from theoretical works. They suggest that the volume density of active SMBHs is relevant at high-z, with several predictions lying above the observed luminosity function of AGNs at these redshifts. For example, predictions from GAEA (Fontanot et al. 2020; De Lucia et al. 2024) or the Rome SAM (Menci et al. 2014) are above the observed fit of the $z = 4$ AGN luminosity function at the faint end, as shown in Figure 4 of Boutsia et al. (2021), but are consistent with the observed bright end. In a similar way, the CAT semi-analytical model (Trinca et al. 2022, 2023) predicts more bright QSOs than the ones observed at $z > 4$. At such high redshifts, these results have deep implications for the proposed SMBH seeding mechanisms (which somehow represent the initial conditions for gas accretions in these models). Mismatch between predictions and observations suggests that seeding mechanisms should be revised accordingly. On the opposite sides, results from the DELPHI semi-analytic model (Dayal et al. 2024) seem to indicate that AGNs are only able to provide about 23% of the total reionization budget and that their space densities are only relevant at $z < 7$, at the end stages of the reionization process. Recent results from Fujimoto et al. (2023) at $z \sim 10$ are one order of magnitude above the predictions of the DELPHI model, possibly indicating that their model cannot easily reproduce the observed AGN luminosity function at high-z. It is worth noting here that a simple model, aimed at reproducing the $z \sim 6$ BH mass–σ relation with overmassive SMBHs with respect to the local relations, would naturally predict abundant AGNs at $z > 7$, as has been recently observed by, for example, Fujimoto et al. (2023), Harikane et al. (2023), Furtak et al. (2024), Greene et al. (2024), Kocevski et al. (2024), and Kokorev et al. (2024).

In order to assess the role of active SMBHs at high-z in the cosmic reionization, we revisit in this work the AGN luminosity function at $z \sim 5$ by combining the results on the bright side from ground-based wide surveys (Grazian et al. 2022, 2023) with the deep pencil-beam surveys from JWST at the faint side.

Table 1
The QSO Space Densities at $z \sim 5$ Adopted in This Work

Survey	z_{spec}	M_{1450}	Φ	$+1\sigma_\Phi$	$-1\sigma_\Phi$	Reference
QUBRICS	4.75	−28.6	3.12E-10	1.08E-10	8.25E-11	Grazian et al. (2022)
RUBICON	4.85	−27.0	1.32E-8	1.29E-8	7.31E-9	Grazian et al. (2023)
RUBICON	4.85	−27.1	8.80E-9	4.76E-9	3.27E-9	Grazian et al. (2023)
Glikman	4.85	−26.0	7.65E-8	1.02E-7	5.06E-8	This paper
CANDELS	5.50	−22.3	1.29E-6	1.72E-6	0.85E-6	Grazian et al. (2020)
G19	5.60	−19.0	7.27E-6	7.12E-6	4.02E-6	Giallongo et al. (2019)
G19	5.60	−20.0	4.77E-6	3.79E-6	2.31E-6	Giallongo et al. (2019)
CEERS	5.00	−19.8	1.07E-5	2.48E-5	9.25E-6	Kocevski et al. (2023)
H23	4.91	−21.5	1.20E-5	0.00E-5	1.20E-5	Harikane et al. (2023)
H23	4.91	−18.5	1.40E-4	1.90E-4	1.40E-4	Harikane et al. (2023)
H23	5.76	−21.5	3.50E-6	8.20E-6	3.30E-6	Harikane et al. (2023)
H23	5.76	−18.5	1.50E-4	3.50E-4	1.50E-4	Harikane et al. (2023)
M24	5.00	−20.0	0.87E-5	0.39E-5	0.37E-5	Matthee et al. (2024)
M24	5.00	−19.0	1.66E-5	0.58E-5	0.54E-5	Matthee et al. (2024)
M24	5.00	−18.0	1.05E-5	0.43E-5	0.43E-5	Matthee et al. (2024)
G24	5.50	−19.5	3.00E-5	0.60E-5	0.60E-5	Greene et al. (2024)
G24	5.50	−19.0	2.10E-5	0.70E-5	0.70E-5	Greene et al. (2024)
G24	5.50	−18.5	2.10E-5	0.80E-5	0.80E-5	Greene et al. (2024)
Mo23	5.00	−18.0	8.71E-4	4.47E-4	3.92E-4	Maiolino et al. (2023)
Mo23	5.00	−19.5	1.48E-4	1.03E-4	0.94E-4	Maiolino et al. (2023)
S24	5.50	−20.15	3.76E-4	2.41E-4	1.57E-4	Scholtz et al. (2023)
S24	5.50	−18.80	7.72E-4	3.85E-4	2.80E-4	Scholtz et al. (2023)
S24	5.50	−17.59	2.17E-3	9.39E-4	7.22E-4	Scholtz et al. (2023)

Note. The AGN space density of Kocevski et al. (2023) adopted here has the errors on Φ, derived through Gehrels (1986) statistics.

The structure of this paper is as follows. In Section 2, we describe the recent AGN luminosity functions at the bright end from wide ground-based surveys and at faint luminosities from JWST. In Section 3, we describe the method we adopt to fit the AGN luminosity functions at $z \sim 5$ and to compute the ionizing emissivity and photoionization rate from active SMBHs. In Section 4, we present our best-fit luminosity function of $z \sim 5$ AGNs, its redshift evolution, a comparison with state-of-the-art semi-analytic models, and the resulting ionizing emissivity and photoionization rate. We critically discuss the outcome of our analysis in Section 5, providing a summary and concluding remarks in Section 6. Throughout the paper, we adopt $H_0 = 70\ \mathrm{km\ s^{-1}\ Mpc^{-1}}$, $\Omega_M = 0.3$, and $\Omega_\Lambda = 0.7$, in agreement with the widely adopted ΛCDM concordance cosmological model. All magnitudes are in the AB photometric system.

2. Data

We present all recent data on $z \sim 5$ QSO and AGN space density estimates that have appeared in the astronomical literature in Table 1. At the bright end ($M_{1450} \leqslant -26$), we consider the results of Grazian et al. (2022) and Grazian et al. (2023) from the QUBRICS and RUBICON surveys, respectively, and the luminosity function derived from the survey of Glikman et al. (2011). In the latter case, we have computed the space density of $z \sim 5$ QSOs by simply dividing the observed number of confirmed QSOs with $4.5 \leqslant z_{spec} \leqslant 5.2$ and $-26.5 \leqslant M_{1450} \leqslant -25.5$ to the cosmological volume of their survey. In an area of 3.76 deg^2, a total of three QSOs have been found by Glikman et al. (2011) in the redshift and luminosity intervals listed above. We assume here a conservative completeness of 100% for this survey, which is slightly higher than the actual values of 66%–80% derived by Glikman et al. (2011) through simulations. The errors on the space density have been derived assuming Gehrels (1986) for low-number statistics. The resulting space density from Glikman et al. (2011) is thus $\Phi = 7.65^{+10.2}_{-5.06} \times 10^{-8}\ cMpc^{-3}\ \mathrm{mag}^{-1}$, as summarized in Table 1.

At faint luminosities ($M_{1450} \geqslant -22.5$), we take into account the data of Giallongo et al. (2019) and Grazian et al. (2020) from the CANDELS survey with HST and all the results from recent JWST surveys (Harikane et al. 2023; Kocevski et al. 2023; Maiolino et al. 2023; Greene et al. 2024; Matthee et al. 2024) for broad-line (Type 1) AGNs. We do not consider here the two brightest points of the Giallongo et al. (2019) luminosity function, since they have been derived with only one object per bin. Similarly, we do not take into account here the $z \sim 5$ AGN luminosity functions of Yang et al. (2016), McGreer et al. (2018), Kulkarni et al. (2019), Kim et al. (2020), Niida et al. (2020), Kim & Im (2021), Finkelstein & Bagley (2022), Jiang et al. (2022), Onken et al. (2022), Pan et al. (2022), Shin et al. (2022), Matsuoka et al. (2023), and Schindler et al. (2023), since they could be severely affected by strong incompleteness, as shown by Grazian et al. (2023).

Recently, Scholtz et al. (2023) showed that the space density of narrow-line (Type 2) AGNs at $z > 4$ is a factor of 2 times larger than the observed density of broad-line (Type 1) AGNs derived by Maiolino et al. (2023). The Type 2-to-Type 1 ratio is around 3 for the brightest AGNs ($M_{1450} = -20.15$) in the JADES survey (Scholtz et al. 2023). These narrow-line AGNs, however, could have a negligible emission of H I ionizing photons (i.e., low values of the escape fraction at $\lambda_{rest} \leqslant 912$ Å along their line of sight). Moreover, their luminosities at 1450 Å rest frame are probably contaminated by the host galaxy light (e.g., Harikane et al. 2023), so it is difficult to properly take into account the contribution of these components to the ionizing emissivity. In the following, we will include the Scholtz et al. (2023) results in our best fit of the AGN luminosity function at $z \sim 5$, but we impose a conservatively low value for the Lyman continuum (LyC) escape fraction of

Table 2
The Different Options for Fitting the AGN Luminosity Functions

Option	Surveys	Comments
Option 1	QUBRICS, RUBICON, Glikman, CANDELS, CEERS, G19, H23, M24, G24	Low luminosity function
Option 2	QUBRICS, RUBICON, Glikman, Mo23	Intermediate luminosity function
Option 3	QUBRICS, RUBICON, Glikman, S24	High luminosity function

Note. For Option 3, the LyC escape fraction of faint AGNs has been fixed to 5%.

this faint population of narrow-line AGNs, as we will discuss in the next sections.

3. Method

3.1. The Best Fit of the AGN Luminosity Function at z ∼ 5

The observed space densities of $z \sim 5$ AGNs (summarized in Table 1) have been fitted with a two-power-law function, leaving free the four parameters, i.e., the faint-end and bright-end slopes α and β as well as the absolute magnitude break M^* and its normalization Φ^*. The parametric best-fit values have been obtained through a minimization of the χ^2 of the observed AGN space densities at $z \sim 5$. Since the values collected in Table 1 are not fully consistent between surveys due to the large variance in AGN space density, especially at the faint end, we identified three main groups of results, called "options" in the following.

The different best-fit options for the observed luminosity functions, summarized in Table 1, are shown in Table 2. We identify three different options for combining the surveys available in the literature: a first conservative option implying the lowest number density of faint Type 1 AGNs, according to the values found in the literature; a second intermediate option, and a third option that maximizes the space densities of faint AGNs, considering both Type 1 and Type 2 AGNs, adopting the results of Scholtz et al. (2023). In all these options, we consider in the bright side ($M_{1450} \leqslant -25$) of the observed luminosity functions the results from the QUBRICS, RUBICON, and Glikman et al. (2011) surveys, shown in Table 1. For the conservative luminosity function (Option 1), we take into account the results of CANDELS (Giallongo et al. 2019; Grazian et al. 2020), CEERS (Kocevski et al. 2023), Harikane et al. (2023), Matthee et al. (2024), and Greene et al. (2024). For the intermediate luminosity function (Option 2), we only consider the recent results of Maiolino et al. (2023) for broad-line (Type 1) AGNs, while for Option 3 (high luminosity function) we take into account the space density of Scholtz et al. (2023).

3.2. Comparison with Theoretical Models

A comparison of the observed $z \sim 5$ AGN luminosity function with model predictions is useful in order to understand the physical properties of the active SMBHs at high-z (e.g., seeding, accretion, feedback, and ionization). Moreover, since observations have limited ranges both in redshifts and in luminosities, theoretical models are useful to fill these gaps and to make quantitative predictions for the AGN population at $z > 6$, where the observations are still limited. We compare here the observed data of the AGN luminosity function at $z \sim 5$ with the recent model predictions by Trinca et al. (2022), Dayal et al. (2024), and De Lucia et al. (2024).

The GAlaxy Evolution and Assembly (GAEA; De Lucia et al. 2024) semi-analytic model follows the evolution of different galaxy populations over cosmological volumes and a wide redshift range, bridging the information of high-z sources to the properties of local galaxies. In this paper, we adopt the latest GAEA version, which couples an explicit partition of the cold gas into atomic and molecular components (Xie et al. 2017), a treatment for the noninstantaneous stripping of cold and hot gas in satellite galaxies (Xie et al. 2020) and an improved modeling for cold gas accretion onto SMBHs and AGN-driven outflows (Fontanot et al. 2020). De Lucia et al. (2024) show that this version of the model, calibrated on the $z < 3$ evolution of the stellar mass function and AGN luminosity function, is able to reproduce the evolution of the fraction and number densities of quenched galaxies up to $z \sim 4$. It also provides comparably large number densities for massive galaxies at $z > 3$ among similar theoretical models, predicting the existence of quenched massive galaxies at $z \sim 6$–7 (Xie et al. 2024). In particular, in this work we consider predictions from a GAEA realization (Fontanot et al. 2024) coupled with merger trees extracted from the P-MILLENNIUM simulation (Baugh et al. 2019), tracking the evolution of the matter distribution over a volume box of 800 comoving megaparsecs on a side. A more thorough analysis of the properties of the highest-z galaxies and AGNs, especially in terms of their predicted UV luminosities as seen by JWST, will be presented in a forthcoming work (S. Cantarella et al. 2024, in preparation).

The DELPHI semi-analytic model (Dayal et al. 2024) recovers the physical properties of early star-forming galaxies and AGNs by including the impact of reionization feedback in the suppression of the baryonic content of low-mass galaxies in ionized regions. DELPHI is able to track the buildup of dark matter halos and their baryonic components, in terms of gas, stellar, dust, metal masses, and black holes, from $z \sim 40$ to $z = 4.5$, over a cosmological volume of 240 comoving megaparsecs on a side. The free parameters of the model (including heavy seeding mechanisms and high accretion rates) are obtained by matching the faint- and bright-ends of the Lyman-break galaxy (LBG) UV luminosity function at $z \sim 5$–9 and the number density of JWST-detected AGNs at $z \sim 5$–7, in addition to the stellar and black hole mass functions and the AGN bolometric luminosity function. By construction, the DELPHI semi-analytic model provides an AGN luminosity function at 1450 Å rest frame that is in good agreement with the observations at $z \sim 5$–7 (including the recent outcome from JWST).

The CAT semi-analytic model (Trinca et al. 2022, 2023) follows the coevolution of star formation and nuclear accretion at $z \geqslant 4$, starting from the formation of the first stars and BHs in a self-consistent way. The free parameters of the CAT model have been tuned to reproduce the observed properties of high-redshift QSOs at $z \geqslant 5$ (SMBH mass and bolometric luminosity functions), the cosmic star formation history and stellar mass density from $z = 4$ to $z = 8$. In the following, we will compare

Table 3
The Best Fit of the z = 5 AGN Luminosity Function and the Corresponding Emissivities and Photoionization Rate

Option	log(Φ*)	M^*	α	β	ϵ_{1450} 10^{24} erg s^{-1}	ϵ_{912} 10^{24} erg s^{-1}	$\Gamma_{\rm H\,I}$ 10^{-12} s^{-1}
Option 1	$-5.60^{+1.15}_{-1.08}$	$-24.57^{+4.56}_{-1.37}$	$-1.32^{+1.01}_{-0.31}$	$-3.46^{+0.43}_{-1.07}$	$12.71^{+4.99}_{-4.01}$	$7.18^{+2.82}_{-2.26}$	$0.80^{+0.31}_{-0.25}$
Option 2	$-7.14^{+4.44}_{-3.16}$	$-26.40^{+6.40}_{-3.60}$	$-2.22^{+2.22}_{-0.32}$	$-3.70^{+1.08}_{-1.30}$	$22.38^{+34.81}_{-9.00}$	$12.65^{+19.68}_{-5.09}$	$1.41^{+2.19}_{-0.57}$
Option 3	$-4.22^{+1.52}_{-5.12}$	$-23.16^{+3.16}_{-5.52}$	$-1.76^{+1.26}_{-0.80}$	$-3.46^{+0.68}_{-1.54}$	$23.69^{+41.54}_{-21.01}$	$17.86^{+31.31}_{-15.83}$	$1.99^{+3.49}_{-1.76}$

Note. All the quoted errors are at the 1σ level (68.3% confidence level). For Option 3, the LyC escape fraction of faint AGNs at $M_{1450} \geqslant -23.0$ has been fixed to 5%, while it is 100% for brighter sources.

the observed properties of $z \sim 5$ AGNs with the "reference model" of Trinca et al. (2022), with Eddington limit for BH accretion, especially tuned to guarantee a good agreement with the observed QSO population at $z > 5$.

3.3. Derivation of Ionizing Emissivity and Photoionization Rate Produced by $z \sim 5$ AGNs

The H I ionizing emissivity at 912 Å rest frame ϵ_{912} is computed starting from the best fit of the luminosity function of $z \sim 5$ AGNs derived above. Following Lusso et al. (2015), we assume a nonionizing continuum at $\lambda_{\rm rest} \geqslant 912$ Å with a spectral index $\alpha_\nu = -0.61$ and a softening at shorter wavelengths ($\lambda_{\rm rest} < 912$ Å) of $\alpha_\nu = -1.70$. The nonionizing emissivity ϵ_{1450} is derived by integrating the luminosity function of AGNs, multiplied by the luminosity, at 1450 Å rest frame. The integration interval runs from $M_{1450} = -30$ to $M_{1450} = -18$, following the method of Giallongo et al. (2015, 2019) and Boutsia et al. (2021).

The ionizing emissivity ϵ_{912} is derived from the nonionizing emissivity ϵ_{1450} by taking into account the spectral energy distribution of Lusso et al. (2015). The H I photoionization rate Γ_{HI} is derived by adopting Equation (11) of Lusso et al. (2015), multiplied by an additional factor of 1.2 in order to take into account the radiative recombination effect, as explained by D'Aloisio et al. (2018). This formula assumes the evolution of the mean free path for ionizing photons obtained by Worseck et al. (2014).

In the above calculations of ϵ_{912} and $\Gamma_{\rm H\,I}$, an escape fraction of LyC photons of 100% is assumed, together with a spectral slope of $\alpha_\nu = -1.70$ at $\lambda_{\rm rest} < 912$ Å. Recent results by Cristiani et al. (2016), Grazian et al. (2018), and Romano et al. (2019) indicate that the escape fraction is around 75%, when assuming a spectral slope for the AGN continuum emission of $\alpha_\nu = -0.7$, without any softening term. This is almost equivalent to assuming an escape fraction of 100% with a spectral softening similar to the one found by Lusso et al. (2015). In the following, the latter assumption from Lusso et al. (2015) is followed, i.e., $\alpha_\nu = -1.70$ at $\lambda_{\rm rest} < 912$ Å and LyC escape fraction of 100%. For Option 3 only, an escape fraction of 5% is assumed for AGNs fainter than $M_{1450} = -23.0$ since, at these magnitudes, Type 2 AGNs are probably dominating.

4. Results

4.1. The Best-fit Luminosity Function of z ~ 5 AGNs

Table 3 summarizes the parameters of the best-fit luminosity functions for the different options identified in Table 2. The associated error bars correspond to 68.3% confidence limits, or equivalently the 1σ level. Table 3 also summarizes the best fit and 1σ uncertainties for the nonionizing and ionizing emissivities, ϵ_{1450} and ϵ_{912}, respectively, and the photoionization rate $\Gamma_{\rm H\,I}$. Figure 1 shows the observed space densities (blue points and arrows) of $z \sim 5$ AGNs for Option 1 of Table 2, with the derived best-fit luminosity function (thick solid dark green line).

The covariances of the luminosity function parameters at the 1σ level for Option 1 are shown in Figure 2 (black areas in the top and bottom-left panels). The best-fit values are identified by a blue asterisk. The 1σ uncertainties for the photoionization rate $\Gamma_{\rm H\,I}$ are shown in the bottom-right panel of Figure 2, where the best-fit value is indicated by a blue vertical line. Similar versions of Figures 1 and 2 for Options 2 and 3 are shown in the Appendix (Figures 6, 7, 8, and 9, respectively).

In Figure 1, we also compare both observational determinations and our best-fit luminosity function against the predictions of semi-analytic models GAEA (dark red long-dashed curve), DELPHI (magenta short-dashed curve), and CAT (orange dotted–dashed curve). At the bright end ($M_{1450} \leqslant -25$), the GAEA and CAT models (Trinca et al. 2022; De Lucia et al. 2024) recover the observed space densities of bright QSOs. The DELPHI model (Dayal et al. 2024), instead, seems to predict a steeper bright-end slope compared to the observations, but it should be noted that their simulations are limited to $M_{1450} \gtrsim -27$. Moreover, the nonmonotonic trend of these models is possibly indicating that their uncertainties are of the same order of magnitude as the differences with the observed luminosity function. It is thus difficult to conclude that one model is better than the others. On the faint-end side ($M_{1450} \geqslant -23$), all three models are able to reproduce the observed space densities of AGNs (for Option 1, i.e., our conservative luminosity function). In case of an even higher space density of $z \sim 5$ AGNs at low luminosities, in agreement with Maiolino et al. (2023) or Scholtz et al. (2023), i.e., our Options 2 and 3, then the predictions of GAEA, DELPHI, and CAT models will underestimate the faint end of the luminosity function.

The H I photoionization rates $\Gamma_{\rm H\,I}$ in Table 3 cover the interval $0.80–1.99 \times 10^{-12}$s^{-1}, according to the different options in Table 2. In these calculations, we have assumed a LyC escape fraction of 100% for the $z = 5$ AGNs. In Option 3, we assume fesc = 5% for AGNs fainter than $M_{1450} = -23.0$ and 100% at higher luminosities. These values of $\Gamma_{\rm H\,I}$ are in rough agreement with the ones derived by the proximity effects or by the fit of the Lyα forest observed in high-z QSOs. In particular, a recent estimate by Davies et al. (2024) from the XQR30 survey (D'Odorico et al. 2023) gives a photoionization rate of $\Gamma_{\rm HI} = 0.599^{+0.109}_{-0.085}$ (in units of 10^{-12} s^{-1}), which is in agreement with our conservative estimate in Table 3 (Option 1). If a lower value of the LyC escape fraction is assumed (e.g., Micheva et al. 2017; Iwata et al. 2022), then

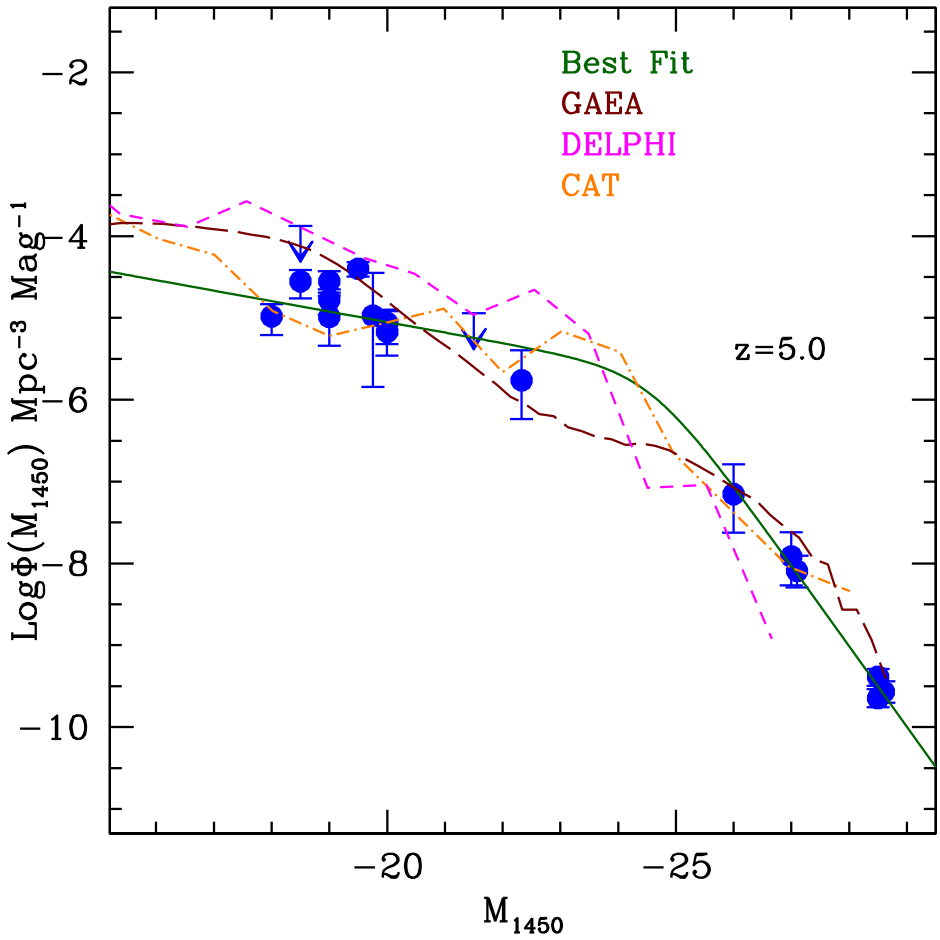

Figure 1. The observed luminosity function of AGNs at $z = 5$ (blue points and arrows), with the best fit (dark green solid line) for Option 1. Comparisons with model predictions by GAEA (De Lucia et al. 2024), DELPHI (Dayal et al. 2024), and CAT (Trinca et al. 2022) are shown by dark red long-dashed, magenta short-dashed, and orange dotted–dashed curves, respectively.

Options 2 is also not far from the Davies et al. (2024) determination. Option 3 gives a large value of $\Gamma_{\rm H\,I}$, three times larger than the XQR30 measurements, but it is worth mentioning that the best fit of the AGN luminosity function has been derived taking into account also the Type 2 AGNs by Scholtz et al. (2023), and that an arbitrary escape fraction of 5% has been adopted at $M_{1450} \geqslant -23.0$ (similar to the values assumed for star-forming galaxies in recent papers). A different (lower) choice for the LyC escape fraction or M_{1450} threshold could result into a better agreement with the Davies et al. (2024) $\Gamma_{\rm H\,I}$. In addition, the uncertainties on the determination of the photoionization rate in the literature are still large, and it is not excluded that $\Gamma_{\rm H\,I}$ could be higher than the present values derived by Gaikwad et al. (2023) or Davies et al. (2024) at $z \sim 5$ by $\sim$0.2 dex, reaching a consistency with Options 2 and 3.

This indicates that with conservative assumptions on the shape of the $z \sim 5$ AGN luminosity function and with the hypothesis that all of these AGNs, from $M_{1450} = -30$ to $M_{1450} = -18$, have a substantial escape fraction of $\sim$100%, then AGNs alone could sustain the ionization of the Universe close to the reionization epoch.

4.2. The Redshift Evolution of the AGN Luminosity Function

Figure 3 shows the evolution of the space densities of bright QSOs and faint AGNs at high-z that recently appeared in the literature. The blue triangles are for UV absolute magnitudes $M_{1450} \leqslant -26.0$ and these space densities have been translated to a magnitude $M_{1450} = -28.0$ following the observed luminosity function, by assuming a bright-end slope of $\beta = -3.46$, as derived from the best fit in Table 3 (for Option 1). Following the same procedures, the green squares are the space densities in the range $-26.0 \leqslant M_{1450} \leqslant -21.0$, and all have been translated to $M_{1450} = -24.0$, assuming a faint-end slope of $\alpha = -1.32$, as found in Table 3 (for Option 1). The red circles are the space densities of AGNs with $M_{1450} > -21.0$, and all have been translated to $M_{1450} = -18.0$, assuming the same faint-end slope of $\alpha = -1.32$.

For each group of space densities ($M_{1450} = -28.0$, $M_{1450} = -24.0$, and $M_{1450} = -18.0$), we compute the best-fit evolution, assuming a linear relation, $\log(\Phi) = \log(\Phi_0) + \gamma(z - z_0)$. The best-fit values for γ are -0.32 ± 0.12, -0.05 ± 0.10, and -0.09 ± 0.08 for $M_{1450} \leqslant -26.0$, $-26.0 \leqslant M_{1450} \leqslant -21.0$, and $M_{1450} > -21.0$, respectively. The observed trend indicates that the evolution of the AGN luminosity function at $z > 3$ is not evolving as a pure space density, as suggested in Grazian et al. (2023) based on the bright side ($M_{1450} \leqslant -28$) of the QSO luminosity functions at $z = 4$ and $z = 5$, but has a differential evolution. While the bright end of the luminosity function is evolving relatively rapidly from $z = 3$ to $z = 6$, at intermediate and faint luminosities the AGN density evolution is slightly

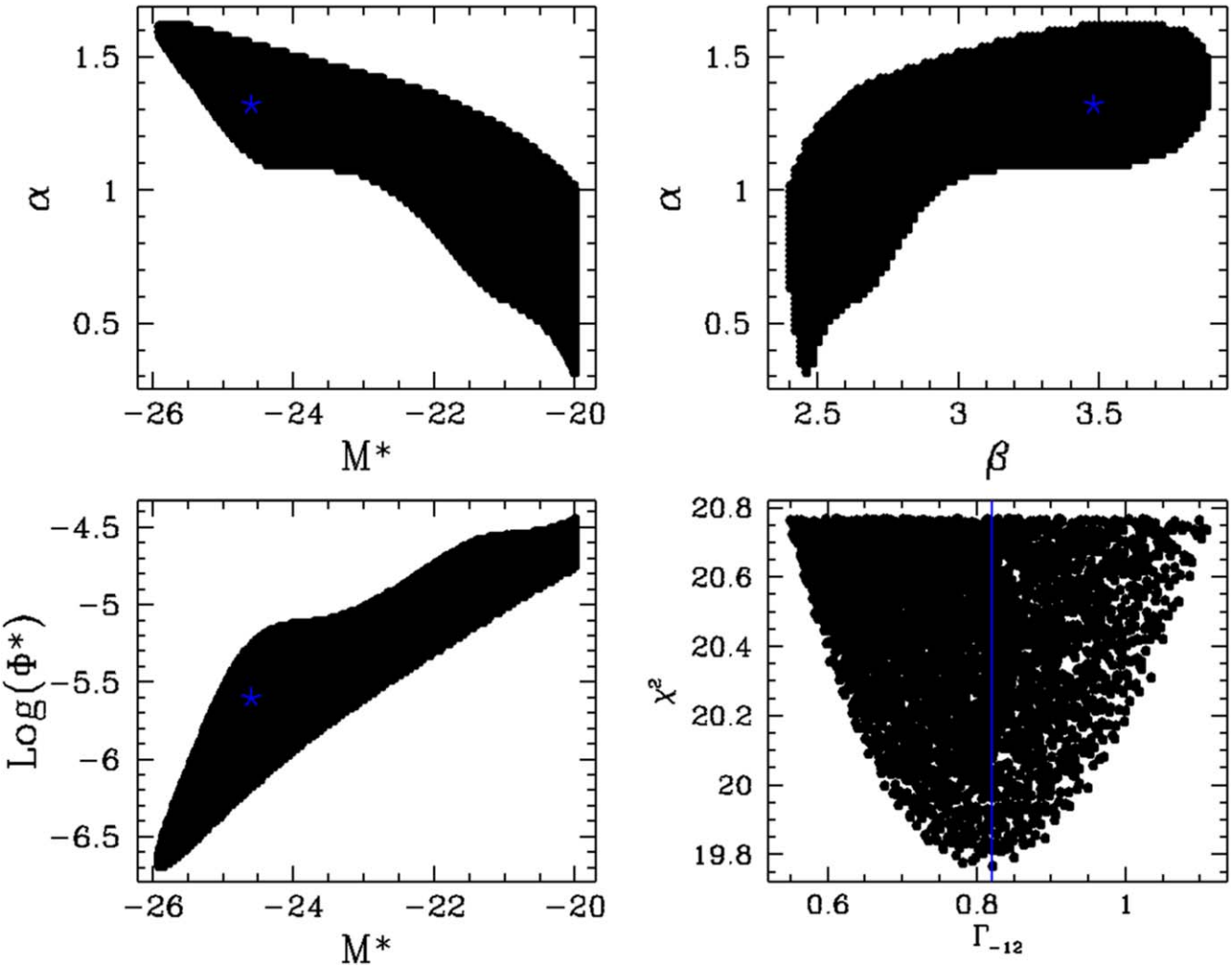

Figure 2. The best-fit luminosity function parameters of AGNs at $z = 5$ for Option 1. The dark areas show the confidence interval at 1σ (68.3% c.l.) for the parameters of the AGN luminosity function at $z \sim 5$. The bottom-right plot shows the permitted interval for the photoionization rate $\Gamma_{\rm H\,I}$ at the 1σ level, while the best-fit value is indicated by the blue vertical line.

milder, consistent with no evolution from $z = 4$ to $z = 10$. If confirmed by future surveys, this differential trend can give stringent constraints on the models for the formation and evolution of the high-z SMBHs and their seeding process (e.g., Trinca et al. 2022).

In Figure 3, we present a comparison with the predictions of the semi-analytic models of Trinca et al. (2022), Dayal et al. (2024), and De Lucia et al. (2024). In general, the three models are able to fairly reproduce the normalization of the AGN space densities at different luminosities for $z \sim 5$. The models considered in this study are facing some difficulties to recover the redshift evolution of the AGN space densities for the intermediate ($M_{1450} \sim -24.0$) luminosities, since they all show a steeper evolution with respect to the observations. If these discrepancies will be confirmed by future observations of faint AGNs at high-z, then a general revision of these theoretical models is probably required. In particular, the BH seeding prescription of the models is particularly sensitive to the space density of high-z AGNs at the faint end. It is also worth pointing out that at the faint end of the AGN luminosity function the contamination from the host galaxy is more probable to have an impact.

5. Discussion

5.1. Differential Evolution of the AGN Luminosity Function?

As shown in Figure 3, the evolution of the faint side of the AGN luminosity function is milder than the one on the bright end. It is possible that this differential evolution is mainly driven by the point at $z = 6$ and $M_{1450} = -28$ by Jiang et al. (2016), where the completeness correction could be underestimated, as also found at lower redshifts by Schindler et al. (2019a, 2019b), Boutsia et al. (2021), and Grazian et al. (2023). If we exclude from the fit of the blue triangles in Figure 3 the point at $z = 6$, the resulting slope is then $\gamma = -0.28 \pm 0.13$, similar to the value derived by Grazian et al. (2022) of $\gamma = -0.25$, and still compatible with the value derived here of $\gamma = -0.32 \pm 0.12$, when the latter point by Jiang et al. (2016) is included. This result probably hints at a differential evolution of the AGN luminosity function between the bright side, evolving with redshift, and the faint side, where it remains almost constant from $z = 4$ to $z = 10$, but better data are needed before supporting these conclusions.

As discussed in Section 4.2, the points in Figure 3 have been shifted to $M_{1450} = -28$, -24 and -18 by adopting the bright-

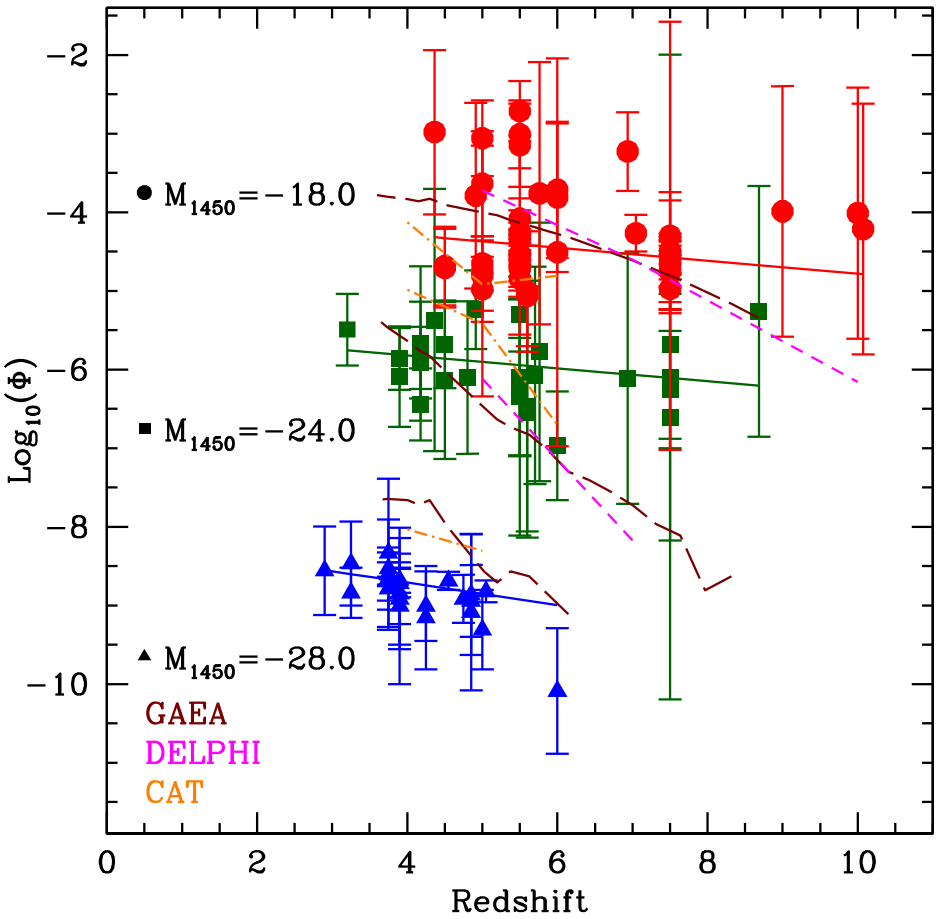

Figure 3. The evolution of the space densities of bright QSOs and faint AGNs at high-z, collected from different surveys in the literature. The points at $z \sim 5$ are summarized in Table 1. The blue, green, and red solid lines are the best-fit weighted linear relations to the observed data points. The dark red long-dashed lines, the magenta short-dashed and orange dotted–dashed lines are the model predictions by GAEA (De Lucia et al. 2024), DELPHI (Dayal et al. 2024), and CAT (Trinca et al. 2022), respectively.

and faint-end slopes of the best-fit luminosity function at $z = 5$ derived here for Option 1, i.e., $\alpha = -1.32$ and $\beta = -3.46$, respectively. We have checked that the above results on the space density evolution of the bright and faint AGNs do not change if we assume the best-fit values for Options 2 or 3. The possible differential evolution of the bright and faint side of the AGN space density does not depend on the assumptions on the exact shape of the AGN luminosity function at $z = 5$.

It is worth stressing here that the space densities of faint AGNs have large error bars and show a nonnegligible variance, indicating that more observations are needed in this luminosity regime. If it will be confirmed in the future that the space density of faint AGNs is relatively constant from $z = 4$ to $z = 10$, then this implies that the AGN occupation fraction among distant galaxies is an increasing function of redshift, due to the relatively rapid evolution in redshift of the space density of star-forming galaxies (e.g., Oesch 2020). The numerous presence of faint AGNs among bright high-z galaxies recently found by the JWST spectroscopy up to $z = 10$ (Harikane et al. 2023; Kocevski et al. 2023; Labbé et al. 2023; Scholtz et al. 2023; Xu et al. 2023; Maiolino et al. 2024a; Andika et al. 2024; Furtak et al. 2024; Greene et al. 2024; Kokorev et al. 2024; Kovács et al. 2024) seems to go in this direction, confirming previous results by Giallongo et al. (2015, 2019) and Grazian et al. (2020, 2022, 2023). The almost ubiquitous presence of active SMBHs at the center of star-forming galaxies at very high redshifts could explain the surprisingly slow evolution of the space density of the bright galaxies at $z > 8$ recently derived by deep JWST observations (e.g., Finkelstein et al. 2024). Indeed, the excess of relatively bright galaxies found by JWST at very high-z with respect to the predictions of ΛCDM models (Yung et al. 2024) could be due to the presence of an AGN at their center, making them brighter, more compact, and also causing the derivation of stellar masses and star formation rates from spectrophotometric codes to be less reliable. Not surprisingly, the space density of the high-z bright galaxies by Finkelstein et al. (2024) is of the order of 10^{-4} Mpc^{-3} at $M_{1450} \sim -19$ and 10^{-5} Mpc^{-3} at $M_{1450} \sim -22$, in very good agreement with the AGN space densities plotted in Figure 3. In the future, a careful investigation of the physical engine (star formation versus AGN) powering these bright galaxies at $z > 8$ will be important to check this hypothesis. Vice versa, the host galaxy light can contaminate the UV luminosity of the central AGN leading to an overestimate of the faint-end of the AGN luminosity function.

5.2. Implications on Ionizing Emissivity

If confirmed by future observations, the mild evolution in redshift of the faint side of the AGN luminosity function has deep implications both for the reionization of hydrogen and the search for the progenitors of the SMBHs detected at $z \gtrsim 6$ with masses of 10^9–10^{10} $M_\odot$. As shown in the results above, the

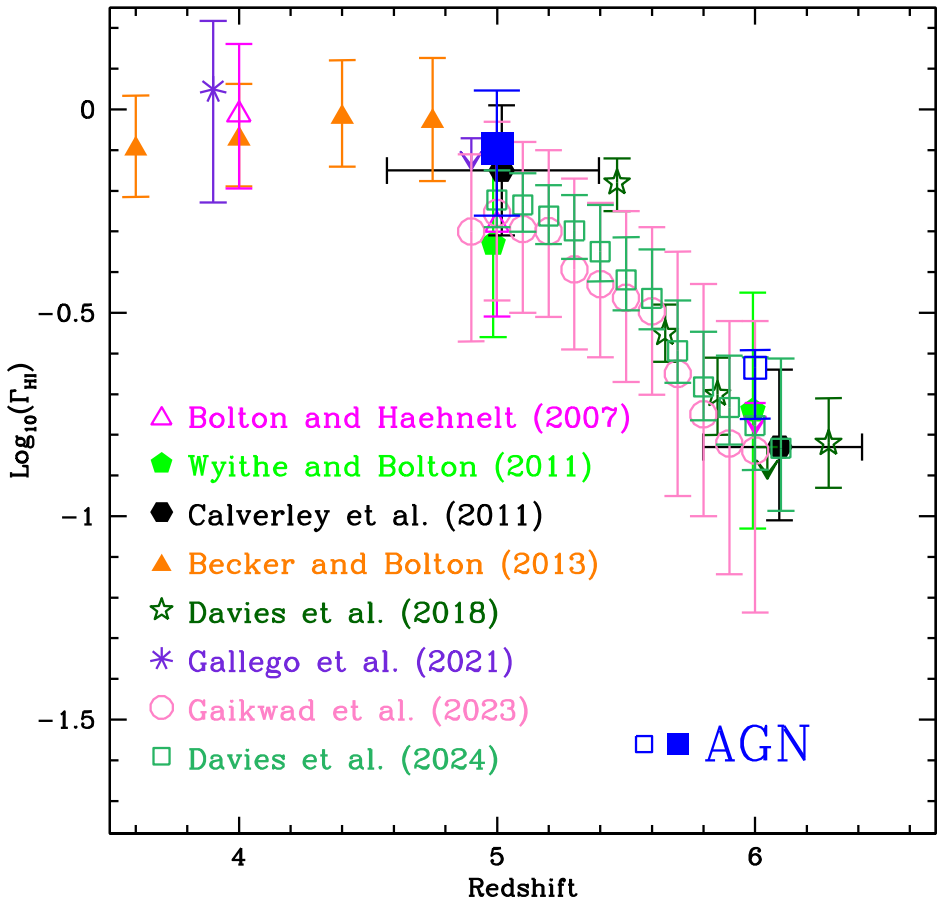

Figure 4. The photoionization rate $\Gamma_{\rm H\,I}$ (in units of 10^{-12} s^{-1}) produced by bright QSOs and faint AGNs at z = 5 (filled blue square, Option 1) and at z = 6 (open blue square). These values have been obtained from the best-fit AGN luminosity function assuming an escape fraction of LyC photons of 100%. All the other points are measurements of the photoionization rate from Lyα forest fitting or from the proximity effect.

population of bright QSOs and faint AGNs at $z \sim 5$ are able to produce an amount of H I ionizing photons comparable with recent estimates of the photoionization rate by the Lyman forest or by the Proximity effect at the end of the reionization epoch, as shown in Figure 4. This agreement suggests a relevant role of AGNs in the process of reionization, as recently proposed by Madau et al. (2024) on the basis of the latest JWST results. This result is in agreement with what has been recently concluded by Fontanot et al. (2023), confirming previous results by Giallongo et al. (2015, 2019). The shape and redshift evolution of the AGN luminosity function at $z \geqslant 5$, moreover, could provide strong constraints on the different scenarios proposed for the formation of the SMBH seeds (Trinca et al. 2022; Fontanot et al. 2023; Trinca et al. 2023; Volonteri et al. 2023; Dayal et al. 2024).

In the calculations of Section 4, we have assumed that the escape fraction of bright QSOs and faint AGNs down to $M_{1450} = -18$ is always 100%. This assumption is not unrealistic, since the observed AGNs at $z > 4$ found by JWST at these luminosities show broad and symmetric Hα lines (e.g., Harikane et al. 2023; Kocevski et al. 2023; Maiolino et al. 2023; Greene et al. 2024; Kokorev et al. 2024), typical of Type 1 AGNs, thus not obscured. Moreover, these objects are showing compact morphologies and blue UV continuum, both typical of unobscured (Type 1) AGNs. This is at odds with the conclusions of, for example, Matthee et al. 2024, hinting at a negligible contribution of these faint AGNs to the ionizing emissivity, due to their possible low LyC escape fraction. Their conclusions about the small fraction of ionizing photons able to escape from these objects are mainly based on their steep slopes in the rest-frame optical, possibly indicating large extinction. However, their spectral slopes in the UV rest frame are relatively flat, hinting at a negligible amount of dust extinction.

At low redshift ($z < 1.5$), the escape fraction of faint ($M_{1450} \sim -19$) AGNs is close to 100%, as shown, for example, by Stevans et al. (2014). The escape fraction of faint ($M_{1450} \lesssim -23$) AGNs at $z \sim 4$ has been studied by Grazian et al. (2018), showing that it is substantial, i.e., ∼70%, over a wide magnitude range. This result has been questioned by Iwata et al. (2022), based on deep u-band imaging of faint AGNs at $z \sim 3$–4. Some of their AGNs, where they estimate a negligible LyC escape fraction, however, are in common with Grazian et al. (2018), where the latter instead find a substantial escape fraction of ionizing photons from deep spectroscopy. This mismatch leaves open the question of the exact value of the escape fraction of faint AGNs at high-z. A more careful investigation of the escape fraction of accreting SMBHs at low luminosity is necessary in the future in order to determine this crucial parameter for estimating the amount of ionizing photons reaching the IGM from high-z, faint AGNs.

Figure 4 shows the strong evolution of the photoionization rate $\Gamma_{\rm H\,I}$ produced by AGNs at $z = 5$ and $z = 6$. The result at $z = 6$ has been derived by a fit of the AGN space density observed at these redshifts (as shown in Figure 3), which could be affected by strong incompleteness or large uncertainties.

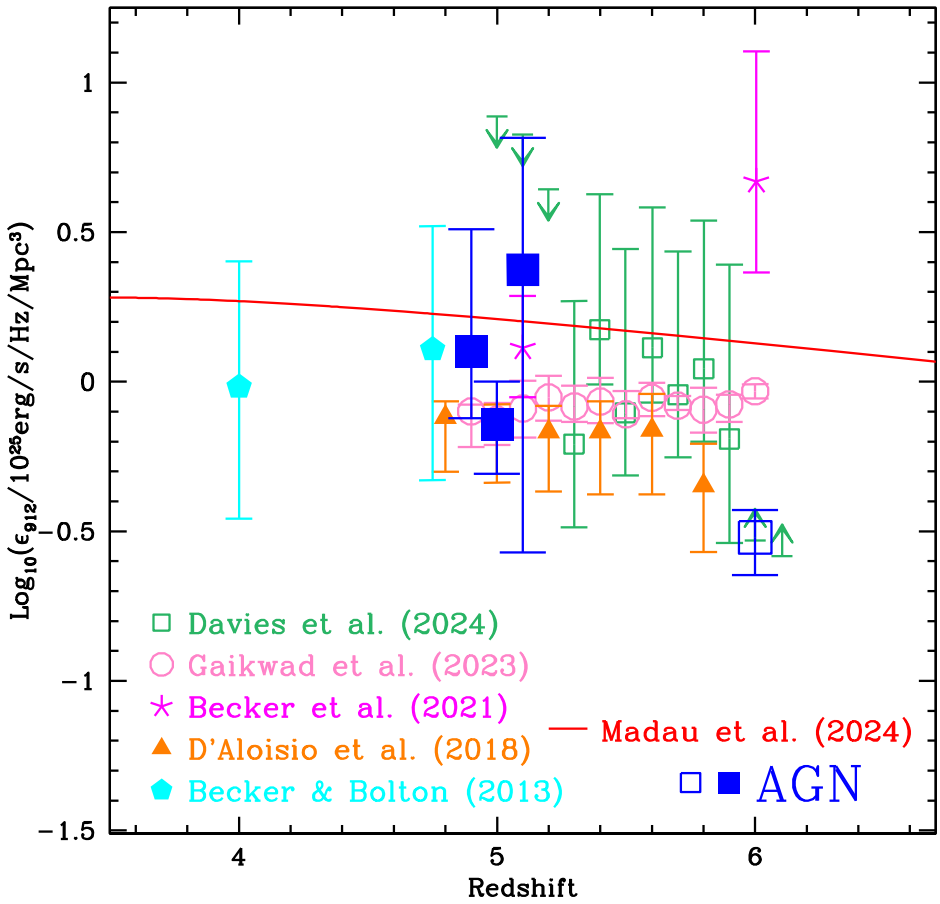

Figure 5. The ionizing emissivity ϵ_{912} (in units of 10^{25} erg s^{-1} Hz^{-1} Mpc^{-3}) produced by bright QSOs and faint AGNs at $z = 5$ (filled blue squares; the lower point represents Option 1, the intermediate value is for Option 2, while the upper point shows the emissivity for Option 3) and at $z = 6$ (open blue square). The emissivities for Options 2 and 3 have been shown by the blue filled squares at $z = 4.9$ and $z = 5.1$, respectively, in order to avoid overlaps in the plot, but they all have been computed at $z = 5$. The red line shows the emissivity adopted by Madau et al. (2024). The other points have been taken from Becker & Bolton (2013), D'Aloisio et al. (2018), Becker et al. (2021), Gaikwad et al. (2023), and Davies et al. (2024).

Moreover, we have used the mean free path of Worseck et al. (2014) at $z = 6$ (almost consistent with the one by Bolton & Haehnelt 2007) to obtain the photoionization rate from the ionizing emissivity ϵ_{912}, but there are possible indications (Becker et al. 2021; Gaikwad et al. 2023; Davies et al. 2024) that the mean free path at $z = 6$ is possibly lower than the one by Worseck et al. (2014). The strong drop of the photoionization rate produced by AGNs from $z = 5$ to $z = 6$ is in slight agreement with the measurements of the ionizing background derived from Lyα forest fitting or from the proximity effect (Bolton & Haehnelt 2007; Calverley et al. 2011; Wyithe & Bolton 2011; Becker & Bolton 2013; Davies et al. 2018; Gallego et al. 2021; Gaikwad et al. 2023; Davies et al. 2024).

In Figure 5, we show the redshift evolution of the ionizing emissivity ϵ_{912} from a collection of recent works (Becker & Bolton 2013; D'Aloisio et al. 2018; Becker et al. 2021; Gaikwad et al. 2023; Davies et al. 2024). For comparison, we add to the plot the emissivity produced by the AGN population at $z = 5$ (for Options 1, 2, and 3) and at $z = 6$. The point at $z = 6$ is still uncertain due to possible incompleteness in the bright side of the AGN luminosity functions at this redshift. From the recent results by Gaikwad et al. (2023), it seems that the ionizing emissivity is flat from $z = 4.5$ to $z = 6$. This implies that the strong drop in the photoionization rate $\Gamma_{\rm H\,I}$ is mainly due to a drop of the mean free path of ionizing photons. Moreover, the constancy of ϵ_{912} is almost consistent with an ionizing emissivity produced by AGNs, where their space density, at least at the faint luminosities, is almost flat, as shown in Figure 3. This is another hint in favor of AGNs possibly being responsible for reionization.

5.3. The Contribution of the Host Galaxy to the Ionizing Emission of AGNs

As discussed in Maiolino et al. (2023) and Scholtz et al. (2023), their observed fluxes are most likely a combination of AGN plus host galaxy light, thus providing an upper limit for the AGN luminosity function for Options 2 and 3. There are, however, hints that the contribution by the host galaxy of these high-z AGNs is negligible. For example, Harikane et al. (2023) find that for 90% of their sample (9 objects out of 10) the point-like central source is a necessary component of the two-dimensional fit of the JWST images, with a typical stellar mass of the host galaxies of $M_{\rm host} \sim 10^{9.5}\ M_{\odot}$. In a similar way, the luminosity of the broad component is dominating (by a factor of 2–5) that of the narrow component in 40% of their sample, it is almost comparable (factor 0.6–0.9) for 20% of their sample, while it is only a factor of 0.2–0.3 for the remaining 40% of their sample. The small sample by Harikane et al. (2023) of 10 objects only, however, could be affected by large variance due to small number statistics. In the future, larger samples of AGN hosts are required to address this issue.

In addition, their estimated SMBH masses are 0.01–0.1 times the stellar mass of their host galaxies, thus implying that the central engine is accreting close to its Eddington limit. In the case of the two AGNs by Kocevski et al. (2023), the light is dominated by the central point-like sources. All these observations indicate that the emissivity of the AGN host galaxy is not the dominant contribution even at the faint side of the AGN luminosity function studied in this work, i.e., at $M_{1450} \sim -18$. Moreover, almost all of the Little Red Dots recently found by JWST (e.g., Kocevski et al. 2023; Barro et al. 2024; Kocevski et al. 2024; Kokorev et al. 2024; Pérez-González et al. 2024) show compact morphologies, blue slopes of their UV rest-frame SEDs, and Balmer lines dominated by the broad component. These are all strong indications that these AGNs are of Type 1, thus their UV light is by far dominated by the nuclear component, with a small contribution by their host galaxies.

It is indeed possible that the central SMBHs are cleaning the surrounding medium during their active phases, leaving also the subdominant stellar ionizing light from the host galaxy free to escape from the interstellar medium (ISM), with a different (softer) spectral shape. This possibility is mentioned by Fiore et al. (2023) to explain the great number of blue "super-Eddington" objects recently discovered by JWST.

5.4. The Possible Issues of a Reionization Process Driven by AGNs

Reionization driven by faint AGNs and bright QSOs has three main apparent issues:

1. If AGNs are able to produce the whole ionizing radiation to ionize the Universe, what is the role of star-forming galaxies? They are much more numerous than AGNs, and even assuming a low escape fraction (∼10%), their additional contribution can exceed the observed emissivity at high-z.
2. A large number of AGNs at high-z would overproduce the X-ray background (Padmanabhan & Loeb 2023).
3. A dominant population of AGNs at high-z would ionize the He II too early (coeval with H I and He I reionization; see, e.g., Garaldi et al. 2019), while the observed epoch for He II reionization is at $z \sim 3$ (Worseck et al. 2019; Makan et al. 2021, 2022).

The first item is not a serious problem. As we have discussed in the above sections, the star-forming galaxies that have been confirmed as LyC emitters at $z > 3$ are relatively rare, of the order of ∼1% of the total galaxy population at that epochs (e.g., Kerutt et al. 2024), and they have large values of the ionizing escape fraction, of the order of 100%. It is thus not surprising if these few leakers would be confirmed to be AGNs, as happened for peculiar sources like GDS3073 (Grazian et al. 2020; Barchiesi et al. 2023; Übler et al. 2023) or for Green Pea analogs, which seem to be powered by luminous X-ray sources (Singha et al. 2024). The recent finding of broad Balmer lines on typical star-forming galaxies, thus hinting at their AGN nature (e.g., Harikane et al. 2023; Labbé et al. 2023; Maiolino et al. 2024a; Furtak et al. 2024; Greene et al. 2024), may point to the fact that the few leakers found among the star-forming galaxy population all could be in fact powered by an AGN. Further spectroscopic analysis with JWST of the confirmed leakers would clarify their nature and could corroborate or refute this hypothesis.

The other two issues, i.e., overproduction of the X-ray background and too-early He II reionization, have been extensively discussed in Madau et al. (2024), where it has been shown that the internal absorption expected for AGNs at 4 Rydberg will delay the He II reionization until $z \sim 3$, as also found by Madau & Haardt (2015) and Basu et al. (2024) and in agreement with recent observations of the He II Lyman forest (e.g., Worseck et al. 2019; Makan et al. 2021, 2022). The faint AGN population recently detected by JWST does not produce an excess of the X-ray background, since they show very few detections in the rest-frame hard X-ray, as shown by, for example, Maiolino et al. (2024b) and Kocevski et al. (2024).

Summarizing, the three apparent issues above are not critical show-stoppers for the AGN-driven reionization scenario we are proposing in this work.

5.5. Future Prospects

As shown in Table 1, the present-day determination of the QSO/AGN luminosity functions at $z \sim 5$ does not cover the intermediate luminosities ($-25.5 \leqslant M_{1450} \leqslant -22.5$), where the bulk of ionizing photons are expected to be produced (see, e.g., Giallongo et al. 2019). Several attempts to fill this gap resulted in very low space densities of AGNs (e.g., Yang et al. 2016; McGreer et al. 2018; Kim et al. 2020; Niida et al. 2020; Kim & Im 2021; Finkelstein & Bagley 2022; Jiang et al. 2022; Shin et al. 2022; Matsuoka et al. 2023; Schindler et al. 2023), but as discussed in Grazian et al. (2023), it is possible that these surveys are strongly affected by severe incompletenesses. The fact that even the most conservative results from JWST (e.g., Matthee et al. 2024) are finding an order of magnitude more AGNs than the above surveys, provides another indication that the former are strongly incomplete. In the future, it is fundamental to extend the search for $z \geqslant 5$ AGNs in the intermediate luminosity regime ($M_{1450} \sim -24$). This will be possible both by extending the present wide surveys (e.g., RUBICON; Grazian et al. 2023) to two or three magnitudes fainter and by enlarging the sky area covered by deep JWST spectroscopy of the $H\alpha$ line with NIRSpec, thus extending the statistics of relatively bright AGNs ($M_{1450} \sim -24$).

Moreover, a leap forward to the AGN space density at high-z will be provided by the Euclid mission (Euclid Collaboration et al. 2019; Laureijs et al. 2020; Euclid Collaboration et al. 2024). It is expected that the deep near-infrared and optical imaging of the Euclid Wide Survey will be instrumental in finding approximately 100 QSOs at $7 < z < 9$ and much more at $z \sim 5$ and at $M_{1450} \sim -24$. With these new QSOs, the break of the AGN luminosity function will be well constrained, leaving the LyC escape fraction as the only unknown parameter to determine the contribution of AGNs to the ionizing background. Dedicated observations in the rest-frame UV will thus be fundamental to close this exercise at $z \sim 5$.

6. Summary and Conclusions

The recent measurements of the space densities of bright QSOs and faint AGNs at $z \sim 5$ trigger a revision of the AGN luminosity function at these cosmological epochs, with a refinement of their contribution to the hydrogen reionization.

We have collected all the recent QSO/AGN luminosity functions at $z\sim5$, discarding those that are severely affected by incompleteness. At the bright end, the space density of $M_{1450}\leqslant-26$ QSOs is well determined, thanks to large area surveys (Grazian et al. 2022), deep imaging (Grazian et al. 2023), and efficient selection criteria, possibly based on machine learning techniques (e.g., Guarneri et al. 2022; Calderone et al. 2024). On the faint side, the space densities of $M_{1450}\geqslant-22$ AGNs have been constrained by JWST deep spectroscopy, finding that the number of active SMBHs at $z\sim5$ is much larger than previous estimates (e.g., Kocevski et al. 2023; Maiolino et al. 2023). The scatter on the number densities at such low luminosities is still large, mainly due to the uncertainties on the identification of faint AGNs among the sample of high-z galaxies and to the scanty number statistics of the first JWST surveys. Future works with JWST would hopefully reduce the variance statistics on the faint side of the AGN luminosity function at $z>5$. The knee of the $z\sim5$ QSO luminosity function ($M_{1450}\sim-24$) is presently undetermined and wide/deep imaging surveys (e.g., Euclid, Rubin, Roman) will be instrumental in filling this gap.

We have carried out a comparison of the observed AGN luminosity function at $z=5$ with three state-of-the-art theoretical models of galaxy and AGN evolution, i.e., GAEA (De Lucia et al. 2024), DELPHI (Dayal et al. 2024), and CAT (Trinca et al. 2022). All three models are able to reproduce the observed space densities of faint AGNs at $M_{1450}\geqslant-23$, while on the bright side ($M_{1450}\leqslant-25$) only GAEA and CAT are able to recover the observed bright-end slope of the QSO luminosity function at $z=5$ (Figure 1). The predicted AGN space density evolution from $z\sim3$ to $z\sim10$ by GAEA, DELPHI, and CAT (Figure 3) appears to be too fast with respect to the observational constraints at $M_{1450}\sim-24$ (e.g., Lai et al. 2024).

We consider three options for fitting the AGN luminosity function at $z\sim5$. A first, conservative, option includes the lowest space densities from JWST at $M_{1450}\geqslant-22$, namely Giallongo et al. (2019), Grazian et al. (2020), Harikane et al. (2023), Kocevski et al. (2023), Greene et al. (2024), and Matthee et al. (2024). Option 2 results in an intermediate estimate for the AGN luminosity function, adopting the larger space density of AGNs by Maiolino et al. (2023). Finally, only for a consistency check, we consider the high luminosity function of Scholtz et al. (2023; Option 3), which includes also Type 2 AGNs. At the bright end, we always consider the luminosity functions of Glikman et al. (2011) and Grazian et al. (2022, 2023) for all three options.

The fit to the AGN space densities has been carried out with a two-power-law parameterization of the luminosity function. The covariance between the four parameters of the AGN luminosity function has been taken into account in order to produce realistic error bars for the output physical quantities. The emissivity at 1450 Å rest-frame ϵ_{1450} has been derived by integrating the luminosity function in the interval $-30<M_{1450}<-18$, where the bulk of the production of the luminosity density is expected. The ionizing emissivity at 912 Å rest-frame ϵ_{912} has been calculated starting from ϵ_{1450} by assuming an AGN spectral slope of $\alpha_\nu=-1.7$, in agreement with Lusso et al. (2015), and a LyC escape fraction of 100%. This is fully equivalent to the assumption of a harder spectral slope of $\alpha_\nu=-0.7$ (Cristiani et al. 2016) with a LyC escape fraction of ∼70% (Grazian et al. 2018; Romano et al. 2019). The photoionization rate $\Gamma_{\rm H\,I}$ has been obtained from ϵ_{912} and from the mean free path of H I ionizing photons at $z\sim5$ by Worseck et al. (2014), which is consistent with the one derived by Gaikwad et al. (2023). The errors on these parameters have been propagated from the covariances of the AGN luminosity functions, as shown in Figure 2.

The resulting best-fit to the AGN luminosity function for the three options has been summarized in Table 3. The ionizing emissivity ϵ_{912} and photoionization rate $\Gamma_{\rm H\,I}$ have been compared to the UV background measured in the Lyα forest or by the proximity effects and it turns out to be fully consistent at $z\sim5$ even if we adopt the most conservative luminosity function (Option 1; see Figures 4 and 5). A preliminary derivation of ϵ_{912} and $\Gamma_{\rm H\,I}$ for AGNs at $z\sim6$ is consistent with the UV background measurements at this redshift, even if more data are required to confirm this result. The agreement of the photoionization rate produced by AGNs at $z\sim5$–6 with the literature values indicates that faint AGNs (and bright QSOs) could be the main drivers of the reionization event that is rapidly taking place at these redshifts. The agreement of $\Gamma_{\rm H\,I}$ produced by AGNs at $z\sim5$ indicates that most probably the contribution of star-forming galaxies to the ionizing background could be subdominant at this redshift (see, e.g., Madau et al. 2024).

A possible major role of high-z AGNs to the reionization process could also be corroborated by the differential redshift evolution of the AGN space densities at different luminosities, as shown in Figure 3. If future data would confirm that the space density of faint AGNs ($M_{1450}\sim-18$) is almost constant from $z\sim4$ to 10 and beyond, then it is plausible that these AGNs have a key role in reionizing the cosmological neutral hydrogen. This constant space density can also naturally explain the excess of $M_{1450}\geqslant-22$ galaxies at very high-z observed by JWST (e.g., Finkelstein et al. 2024), without any crisis for the ΛCDM model.

In the near future, the faint end of the AGN luminosity function at $z>5$ will be addressed by deep JWST spectroscopy, while the knee of the AGN luminosity function will be constrained by upcoming wide and deep surveys, e.g., Euclid Wide/Deep Surveys, Vera Rubin LSST, and Roman Space Telescope. With these next generation surveys it will be possible to check whether AGNs could be the long-sought pillars of reionization. Time is thus promising for huge progresses in the fields of cosmic reionization and SMBH evolution.

Acknowledgments

We warmly thank the referee for the comments that allowed us to significantly improve the quality of this paper.

We acknowledge the support of the INAF GO/GTO Grant 2023 “Finding the Brightest Cosmic Beacons in the Universe with QUBRICS” (PI: Grazian).

A.G., A.B., and I.S. acknowledge the support of the INAF Mini Grant 2022 “Learning Machine Learning techniques to dig up high-z AGN in the Rubin-LSST Survey.”

A.G. acknowledges the PRIN 2022 project 2022ZSL4BL INSIGHT, funded by the European UnionNextGenerationEU RFF M4C2 1.1.

We acknowledge financial contribution from the grant PRIN INAF 2019 (RIC) 1.05.01.85.09: “New light on the Intergalactic Medium (NewIGM).”

A.G. and F.F. acknowledge support from PRIN MIUR project "Black hole winds and the Baryon Life Cycle of Galaxies: the stone-guest at the galaxy evolution supper," contract 2017-PH3WAT.

The work of K.B. is supported by NOIRLab, which is managed by the Association of Universities for Research in Astronomy (AURA) under a cooperative agreement with the U.S. National Science Foundation.

Appendix
The AGN Luminosity Functions and Their Best-fit Parameterization

Figures 6, 7, 8, and 9 show the collections of the $z \sim 5$ AGN luminosity functions for Options 2 and 3, as summarized in Table 2, the resulting best-fit parameters, and their covariance errors, respectively.

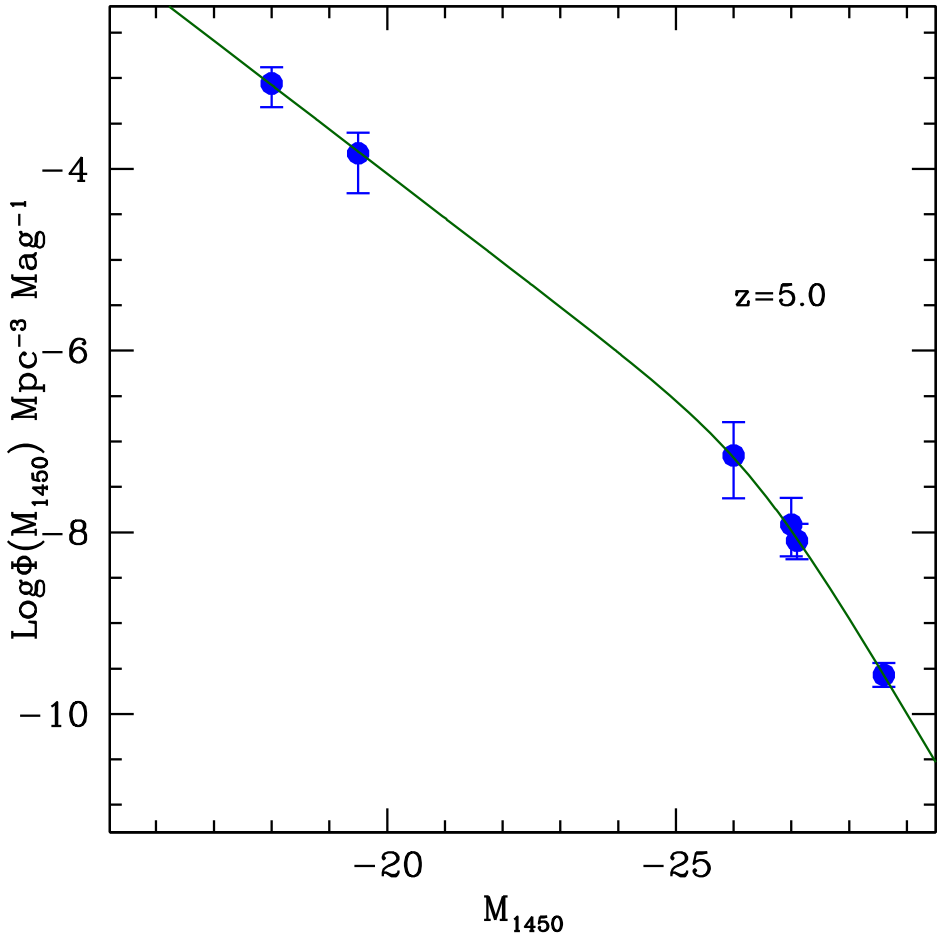

Figure 6. The observed luminosity function of AGNs at $z = 5$ (blue points), with the best fit (green line) for Option 2.

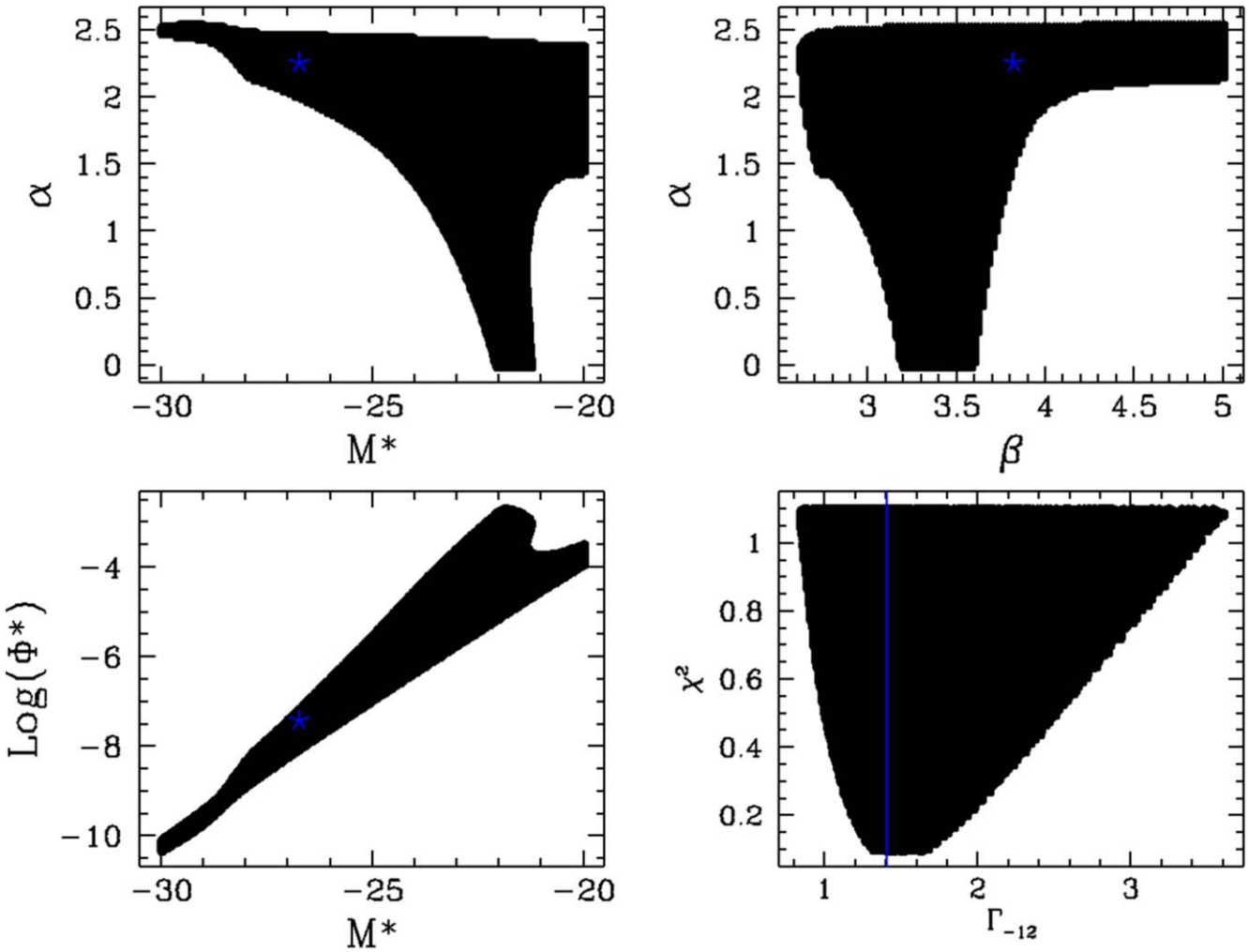

Figure 7. The best-fit luminosity function parameters of AGNs at z = 5 for Option 2. The dark areas show the confidence interval at 1σ (68.3% c.l.) for the parameters of the AGN luminosity function at $z \sim 5$. The bottom-right plot shows the permitted interval for the photoionization rate Γ_{-12} at the 1σ level.

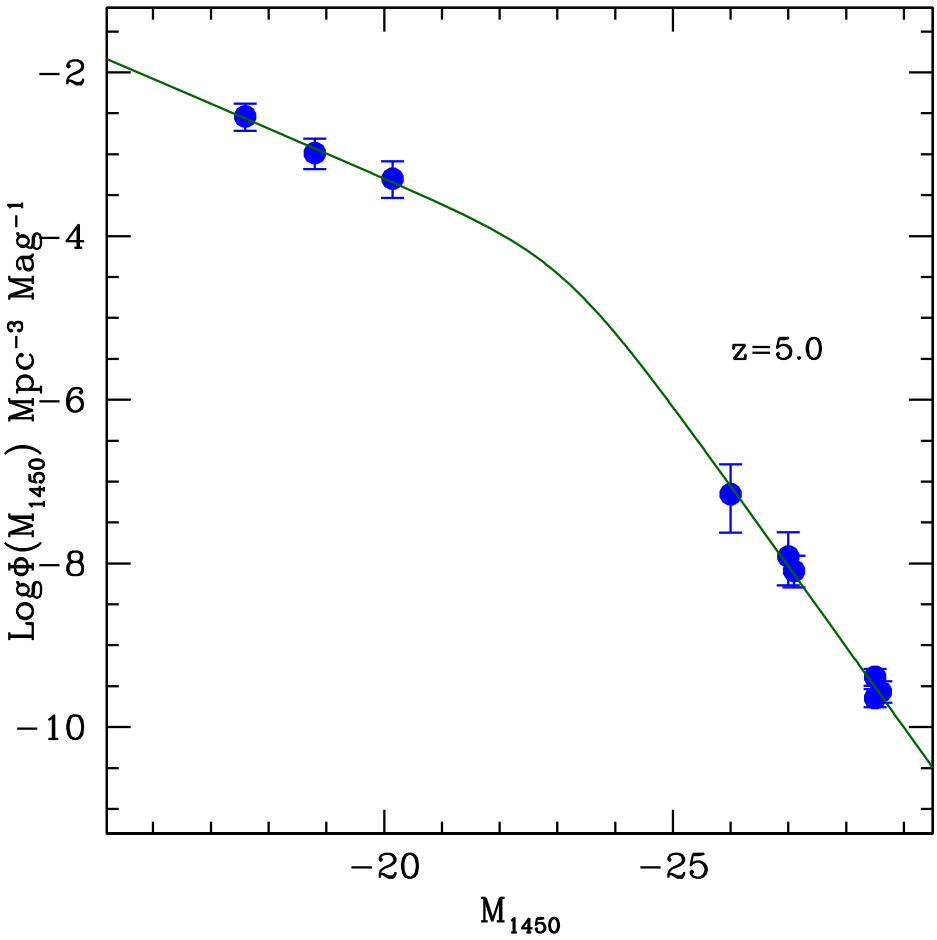

Figure 8. The observed luminosity function of AGNs at $z = 5$ (blue points), with the best fit (dark green line) for Option 3.

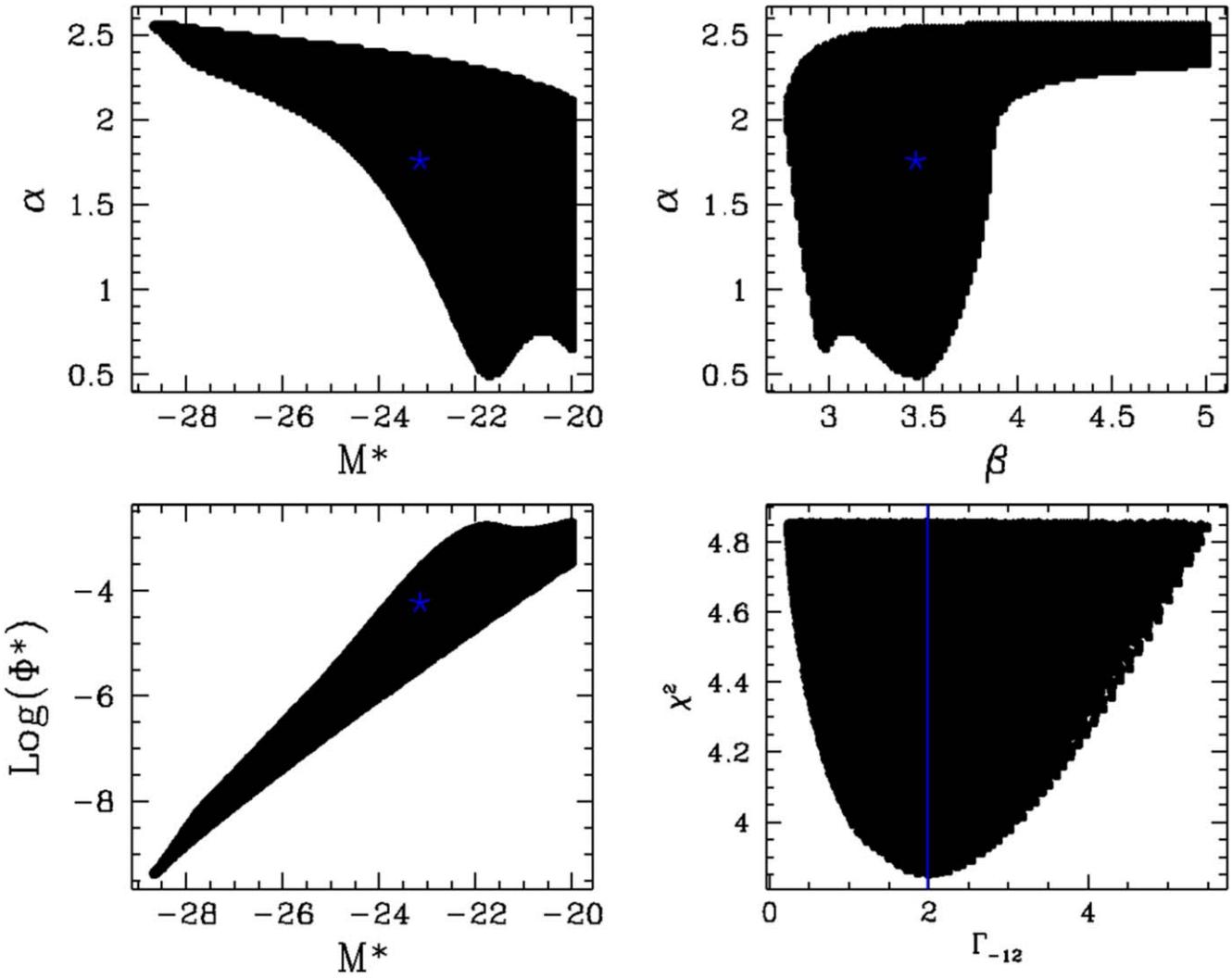

Figure 9. The best-fit luminosity function parameters of AGNs at $z = 5$ for Option 3. The dark areas show the confidence interval at 1σ (68.3% c.l.) for the parameters of the AGN luminosity function at $z \sim 5$. The bottom-right plot shows the permitted interval for the photoionization rate Γ_{-12} at the 1σ level.

ORCID iDs

Andrea Grazian https://orcid.org/0000-0002-5688-0663
Emanuele Giallongo https://orcid.org/0000-0003-0734-1273
Konstantina Boutsia https://orcid.org/0000-0003-4432-5037
Stefano Cristiani https://orcid.org/0000-0002-2115-5234
Fabio Fontanot https://orcid.org/0000-0003-4744-0188
Manuela Bischetti https://orcid.org/0000-0002-4314-021X
Laura Bisigello https://orcid.org/0000-0003-0492-4924
Angela Bongiorno https://orcid.org/0000-0002-0101-6624
Giorgio Calderone https://orcid.org/0000-0002-7738-5389
Francesco Chiti Tegli https://orcid.org/0009-0001-7950-2892
Guido Cupani https://orcid.org/0000-0002-6830-9093
Gabriella De Lucia https://orcid.org/0000-0002-6220-9104
Valentina D'Odorico https://orcid.org/0000-0003-3693-3091
Chiara Feruglio https://orcid.org/0000-0002-4227-6035
Fabrizio Fiore https://orcid.org/0000-0002-4031-4157
Giovanni Gandolfi https://orcid.org/0000-0003-3248-5666
Giorgia Girardi https://orcid.org/0009-0005-6156-4066
Francesco Guarneri https://orcid.org/0000-0003-4740-9762
Michaela Hirschmann https://orcid.org/0000-0002-3301-3321
Matteo Porru https://orcid.org/0009-0004-2597-6146
Giulia Rodighiero https://orcid.org/0000-0002-9415-2296
Ivano Saccheo https://orcid.org/0000-0003-1174-6978
Matteo Simioni https://orcid.org/0000-0002-8830-1259
Andrea Trost https://orcid.org/0000-0002-5959-5964
Akke Viitanen https://orcid.org/0000-0001-9383-786X

References

Adams, N. J., Conselice, C. J., Austin, D., et al. 2024, ApJ, 965, 169
Andika, I. T., Jahnke, K., Onoue, M., et al. 2024, A&A, 685, A25
Atek, H., Labbé, I., Furtak, L. J., et al. 2024, Natur, 626, 975
Barchiesi, L., Dessauges-Zavadsky, M., Vignali, C., et al. 2023, A&A, 675, A30
Barkana, R., & Loeb, A. 2001, PhR, 349, 125
Barro, G., Pérez-González, P. G., Kocevski, D. D., et al. 2024, ApJ, 963, 128
Basu, A., Garaldi, E., & Ciardi, B. 2024, MNRAS, 532, 841
Baugh, C. M., Gonzalez-Perez, V., Lagos, C. D. P., et al. 2019, MNRAS, 483, 4922
Becker, G. D., & Bolton, J. S. 2013, MNRAS, 436, 1023
Becker, G. D., D'Aloisio, A., Christenson, H. M., et al. 2021, MNRAS, 508, 1853
Bogdán, Á., Goulding, A. D., Natarajan, P., et al. 2024, NatAs, 8, 126
Bolton, J. S., & Haehnelt, M. G. 2007, MNRAS, 382, 325
Bosman, S. E. I., Davies, F. B., Becker, G. D., et al. 2022, MNRAS, 514, 55
Boutsia, K., Grazian, A., Fontanot, F., et al. 2021, ApJ, 912, 111
Calderone, G., Guarneri, F., Porru, M., et al. 2024, A&A, 683, A34

Calverley, A. P., Becker, G. D., Haehnelt, M. G., & Bolton, J. S. 2011, MNRAS, 412, 2543
Chardin, J., Puchwein, E., & Haehnelt, M. G. 2017, MNRAS, 465, 3429
Chemerynska, I., Atek, H., Furtak, L. J., et al. 2024, MNRAS, 531, 2615
Chworowsky, K., Finkelstein, S. L., Boylan-Kolchin, M., et al. 2024, AJ, 168, 113
Cristiani, S., Serrano, L. M., Fontanot, F., Vanzella, E., & Monaco, P. 2016, MNRAS, 462, 2478
D'Aloisio, A., McQuinn, M., Davies, F. B., & Furlanetto, S. R. 2018, MNRAS, 473, 560
Davies, F. B., Hennawi, J. F., Bañados, E., et al. 2018, ApJ, 864, 142
Davies, F. B., Bosman, S. E. I., Gaikwad, P., et al. 2024, ApJ, 965, 134
Dayal, P., & Ferrara, A. 2018, PhR, 780, 1
Dayal, P., Volonteri, M., Greene, J. E., et al. 2024, arXiv:2401.11242
De Lucia, G., Fontanot, F., Xie, L., & Hirschmann, M. 2024, A&A, 687, A68
D'Odorico, V., Bañados, E., Becker, G. D., et al. 2023, MNRAS, 523, 1399
Euclid Collaboration, Barnett, R., Warren, S. J., et al. 2019, A&A, 631, A85
Euclid Collaboration, Mellier, Y., Abdurro'uf, et al. 2024, arXiv:2405.13491
Ferrara, A., Pallottini, A., & Dayal, P. 2023, MNRAS, 522, 3986
Finkelstein, S. L., & Bagley, M. B. 2022, ApJ, 938, 25
Finkelstein, S. L., Leung, G. C. K., Bagley, M. B., et al. 2024, ApJL, 969, L2
Fiore, F., Ferrara, A., Bischetti, M., Feruglio, C., & Travascio, A. 2023, ApJL, 943, L27
Fiore, F., Grazian, A., Santini, P., et al. 2008, ApJ, 672, 94
Flury, S. R., Jaskot, A. E., Ferguson, H. C., et al. 2022a, ApJS, 260, 1
Flury, S. R., Jaskot, A. E., Ferguson, H. C., et al. 2022b, ApJ, 930, 126
Fontanot, F., Cristiani, S., & Vanzella, E. 2012, MNRAS, 425, 1413
Fontanot, F., De Lucia, G., Hirschmann, M., et al. 2020, MNRAS, 496, 3943
Fontanot, F., Cristiani, S., Grazian, A., et al. 2023, MNRAS, 520, 740
Fontanot, F., De Lucia, G., Xie, L., et al. 2024, arXiv:2409.02194
Fujimoto, S., Wang, B., Weaver, J., et al. 2023, arXiv:2308.11609
Furtak, L. J., Labbé, I., Zitrin, A., et al. 2024, Natur, 628, 57
Gaikwad, P., Haehnelt, M. G., Davies, F. B., et al. 2023, MNRAS, 525, 4093
Gallego, S. G., Cantalupo, S., Sarpas, S., et al. 2021, MNRAS, 504, 16
Garaldi, E., Compostella, M., & Porciani, C. 2019, MNRAS, 483, 5301
Gehrels, N. 1986, ApJ, 303, 336
George, E. M., Reichardt, C. L., Aird, K. A., et al. 2015, ApJ, 799, 177
Giallongo, E., Menci, N., Fiore, F., et al. 2012, ApJ, 755, 124
Giallongo, E., Grazian, A., Fiore, F., et al. 2015, A&A, 578, A83
Giallongo, E., Grazian, A., Fiore, F., et al. 2019, ApJ, 884, 19
Glikman, E., Djorgovski, S. G., Stern, D., et al. 2011, ApJL, 728, L26
Goulding, A. D., Greene, J. E., Setton, D. J., et al. 2023, ApJL, 955, L24
Grazian, A., Giallongo, E., Boutsia, K., et al. 2018, A&A, 613, A44
Grazian, A., Giallongo, E., Fiore, F., et al. 2020, ApJ, 897, 94
Grazian, A., Giallongo, E., Boutsia, K., et al. 2022, ApJ, 924, 62
Grazian, A., Boutsia, K., Giallongo, E., et al. 2023, ApJ, 955, 60
Greene, J. E., Labbe, I., Goulding, A. D., et al. 2024, ApJ, 964, 39
Guarneri, F., Calderone, G., Cristiani, S., et al. 2022, MNRAS, 517, 2436
Haardt, F., & Madau, P. 1996, ApJ, 461, 20
Haardt, F., & Madau, P. 2012, ApJ, 746, 125
Haardt, F., & Salvaterra, R. 2015, A&A, 575, L16
Habouzit, M. 2024, arXiv:2405.05319
Harikane, Y., Zhang, Y., Nakajima, K., et al. 2023, ApJ, 959, 39
Harvey, T., Conselice, C., Adams, N. J., et al. 2024, arXiv:2403.03908
Hayes, M. J., Tan, J. C., Ellis, R. S., et al. 2024, arXiv:2403.16138
Hegde, S., Wyatt, M. M., & Furlanetto, S. R. 2024, arXiv:2405.01629
Iwata, I., Sawicki, M., Inoue, A. K., et al. 2022, MNRAS, 509, 1820
Jiang, L., McGreer, I. D., Fan, X., et al. 2016, ApJ, 833, 222
Jiang, L., Ning, Y., Fan, X., et al. 2022, NatAs, 6, 850
Jin, X., Yang, J., Fan, X., et al. 2023, ApJ, 942, 59
Jung, I., Ferguson, H. C., Hayes, M. J., et al. 2024, arXiv:2403.02388
Kerutt, J., Oesch, P. A., Wisotzki, L., et al. 2024, A&A, 684, A42
Killi, M., Watson, D., Brammer, G., et al. 2023, arXiv:2312.03065
Kim, Y., & Im, M. 2021, ApJL, 910, L11
Kim, Y., Im, M., Jeon, Y., et al. 2020, ApJ, 904, 111
Kocevski, D. D., Onoue, M., Inayoshi, K., et al. 2023, ApJL, 954, L4
Kocevski, D. D., Finkelstein, S. L., Barro, G., et al. 2024, arXiv:2404.03576
Kokorev, V., Caputi, K. I., Greene, J. E., et al. 2024, ApJ, 968, 38
Kovács, O. E., Bogdán, A. ´, Natarajan, P., et al. 2024, ApJL, 965, L21
Kulkarni, G., Worseck, G., & Hennawi, J. F. 2019, MNRAS, 488, 1035
Labbé, I., van Dokkum, P., Nelson, E., et al. 2023, Natur, 616, 266
Lai, S., Onken, C. A., Wolf, C., Bian, F., & Fan, X. 2024, arXiv:2405.10721
Larson, R. L., Finkelstein, S. L., Kocevski, D. D., et al. 2023, ApJL, 953, L29
Laureijs, R., Racca, G. D., Mellier, Y., et al. 2020, Proc. SPIE, 11443, 114430F
Li, J., Silverman, J. D., Shen, Y., et al. 2024, arXiv:2403.00074
Lusso, E., Worseck, G., Hennawi, J. F., et al. 2015, MNRAS, 449, 4204
Madau, P., Giallongo, E., Grazian, A., & Haardt, F. 2024, arXiv:2406.18697
Madau, P., & Haardt, F. 2015, ApJL, 813, L8
Maiolino, R., Scholtz, J., Curtis-Lake, E., et al. 2023, arXiv:2308.01230
Maiolino, R., Scholtz, J., Witstok, J., et al. 2024a, Natur, 627, 59
Maiolino, R., Risaliti, G., Signorini, M., et al. 2024b, arXiv:2405.00504
Makan, K., Worseck, G., Davies, F. B., et al. 2021, ApJ, 912, 38
Makan, K., Worseck, G., Davies, F. B., et al. 2022, ApJ, 927, 175
Mascia, S., Pentericci, L., Calabrò, A., et al. 2024, A&A, 685, A3
Matsuoka, Y., Onoue, M., Iwasawa, K., et al. 2023, ApJL, 949, L42
Matthee, J., Naidu, R. P., Brammer, G., et al. 2024, ApJ, 963, 129
McGreer, I. D., Fan, X., Jiang, L., & Cai, Z. 2018, AJ, 155, 131
Menci, N., Gatti, M., Fiore, F., & Lamastra, A. 2014, A&A, 569, A37
Micheva, G., Iwata, I., & Inoue, A. K. 2017, MNRAS, 465, 302
Muñoz, J. B., Mirocha, J., Chisholm, J., Furlanetto, S. R., & Mason, C. 2024, arXiv:2404.07250
Naidu, R. P., Oesch, P. A., van Dokkum, P., et al. 2022, ApJL, 940, L14
Niida, M., Nagao, T., Ikeda, H., et al. 2020, ApJ, 904, 89
Oesch, P. 2020, in IAU Symp. 352, Uncovering Early Galaxy Evolution in the ALMA and JWST Era, ed. E. da Cunha et al. (Cambridge: Cambridge Univ. Press), 12
Onken, C. A., Wolf, C., Bian, F., et al. 2022, MNRAS, 511, 572
Padmanabhan, H., & Loeb, A. 2023, ApJL, 958, L7
Pan, Z., Jiang, L., Fan, X., Wu, J., & Yang, J. 2022, ApJ, 928, 172
Pérez-González, P. G., Barro, G., Rieke, G. H., et al. 2024, ApJ, 968, 4
Planck Collaboration, Aghanim, N., Akrami, Y., et al. 2020, A&A, 641, A6
Puchwein, E., Haardt, F., Haehnelt, M. G., & Madau, P. 2019, MNRAS, 485, 47
Reichardt, C. L., Patil, S., Ade, P. A. R., et al. 2021, ApJ, 908, 199
Romano, M., Grazian, A., Giallongo, E., et al. 2019, A&A, 632, A45
Schindler, J.-T., Fan, X., McGreer, I. D., et al. 2019a, ApJ, 871, 258
Schindler, J.-T., Fan, X., Huang, Y.-H., et al. 2019b, ApJS, 243, 5
Schindler, J.-T., Bañados, E., Connor, T., et al. 2023, ApJ, 943, 67
Scholtz, J., Maiolino, R., D'Eugenio, F., et al. 2023, arXiv:2311.18731
Shin, S., Im, M., & Kim, Y. 2022, ApJ, 937, 32
Singha, M., Sarmiento, J., Malhotra, S., et al. 2024, arXiv:2406.18730
Spina, B., Bosman, S. E. I., Davies, F. B., Gaikwad, P., & Zhu, Y. 2024, arXiv:2405.12273
Stevans, M. L., Shull, J. M., Danforth, C. W., & Tilton, E. M. 2014, ApJ, 794, 75
Trinca, A., Schneider, R., Maiolino, R., et al. 2023, MNRAS, 519, 4753
Trinca, A., Schneider, R., Valiante, R., et al. 2022, MNRAS, 511, 616
Übler, H., Maiolino, R., Curtis-Lake, E., et al. 2023, A&A, 677, A145
Volonteri, M., Habouzit, M., & Colpi, M. 2023, MNRAS, 521, 241
Worseck, G., Davies, F. B., Hennawi, J. F., & Prochaska, J. X. 2019, ApJ, 875, 111
Worseck, G., Prochaska, J. X., O'Meara, J. M., et al. 2014, MNRAS, 445, 1745
Wyithe, J. S. B., & Bolton, J. S. 2011, MNRAS, 412, 1926
Xie, L., De Lucia, G., Hirschmann, M., & Fontanot, F. 2020, MNRAS, 498, 4327
Xie, L., De Lucia, G., Hirschmann, M., Fontanot, F., & Zoldan, A. 2017, MNRAS, 469, 968
Xie, L., De Lucia, G., Fontanot, F., et al. 2024, ApJL, 966, L2
Xu, Y., Ouchi, M., Nakajima, K., et al. 2023, arXiv:2310.06614
Yang, J., Wang, F., Wu, X.-B., et al. 2016, ApJ, 829, 33
Yung, L. Y. A., Somerville, R. S., Finkelstein, S. L., Wilkins, S. M., & Gardner, J. P. 2024, MNRAS, 527, 5929
Zhu, Y., Becker, G. D., Bosman, S. E. I., et al. 2022, ApJ, 932, 76
Zhu, Y., Becker, G. D., Bosman, S. E. I., et al. 2024, MNRAS, 533, L49